Marine anoxia initiates giant sulfur-bacteria mat proliferation and associated changes in benthic nitrogen, sulfur, and iron cycling in the Santa Barbara Basin, California Borderland

David J. Yousavich[1*], De'Marcus Robinson[2], Xuefeng Peng[3], Sebastian J. E. Krause[1,4], Frank Wenzhöfer[5,6,7], Felix Janssen[5,6], Na Liu[8], Jonathan Tarn[8], Frank Kinnaman[8], David L. Valentine[8], Tina Treude[1,2*]

[1]Department of Earth, Planetary, and Space Sciences, University of California Los Angeles, 595 Charles E. Young Drive East, Los Angeles, CA 90095, USA

[2]Department of Atmospheric and Oceanic Sciences, University of California Los Angeles, Math Science Building, 520 Portola Plaza, Los Angeles, CA 90095, USA

[3]School of Earth, Ocean, and Environment, University of South Carolina, 701 Sumter Street, EWS 617, Columbia, SC 29208, USA

[4]Earth Research Institute, 6832 Ellison Hall, University of California Santa Barbara, Ca 93106-3060

[5]HGF-MPG Joint Research Group for Deep-Sea Ecology and Technology, Alfred-Wegener-Institute, Helmholtz-Center for Polar and Marine Research, Am Handelshafen 12, 27570 Bremerhaven, Germany

[6] HGF-MPG Joint Research Group for Deep-Sea Ecology and Technology, Max Planck Institute for Marine Microbiology, Celsiusstrasse 1, 28359 Bremen, Germany

[7]Department of Biology, DIAS, Nordcee and HADAL Centres, University of Southern Denmark, 5230 Odense M, Denmark

[8]Department of Earth Science and Marine Science Institute, University of California, Santa Barbara, CA 93106, USA

Correspondence: David Yousavich (yousavdj@ucla.edu), Tina Treude (ttreude@g.ucla.edu)

Abstract

The Santa Barbara Basin naturally experiences transient deoxygenation due to its unique geological setting in the Southern California Borderland and seasonal changes in ocean currents. Long-term measurements of the basin showed that anoxic events and subsequent nitrate exhaustion in the bottom waters have been occurring more frequently and lasting longer over the past decade. One characteristic of the Santa Barbara Basin is the seasonal development of extensive mats of benthic nitrate-reducing sulfur-oxidizing bacteria, which are found at the sediment-water interface when the basin's bottom waters reach anoxia but still provide some nitrate. To assess the mat's impact on the benthic and pelagic redox environment, we collected biogeochemical sediment and benthic flux data in November 2019, after anoxia developed in the deepest waters of the basin and dissolved nitrate was depleted (down to 9.9 μM). We found that the development of mats was associated with a shift from denitrification to dissimilatory nitrate reduction to ammonium. The zone of sulfate reduction appeared near the sediment-water interface in sediment hosting these ephemeral white mats. We found that an exhaustion of iron oxides in the surface sediment was an additional prerequisite for mat proliferation. Our research further suggests that cycles of deoxygenation and reoxygenation of the benthic environment result in extremely high benthic fluxes of dissolved iron from the basin's sediment. This work expands our understanding of nitrate-reducing sulfur-oxidizing mats and their role in sustaining and potentially expanding marine anoxia.

Introduction

Naturally occurring low-oxygen waters in the ocean are commonly observed below the ocean's mixed layer where respiration consumes oxygen faster than it is produced or ventilated. When low oxygen conditions occur along the western continental shelf in regions susceptible to upwelling events and/or undergoing eutrophication, organic matter remineralization can frequently drive oxygen concentrations to hypoxic (O_2 < 63 μM) (Middelburg and Levin, 2009) and/or anoxic levels (O_2 < 3 μM) (Fossing et al., 1995; Canfield et al., 2010). These areas are usually referred to as Oxygen Minimum Zones (OMZs). In the water column of OMZs, nitrogen reduction becomes an important mechanism for organic matter remineralization (Ward et al., 2009). OMZs within coastal basins that experience seasonal changes in upwelling can experience anoxic and nitrate reducing conditions that extend to the benthic environment, especially when high productivity and associated organic matter export coincide with seasonal patterns of physical mixing. This fundamental change in the redox conditions at the sediment-water interface encourages elevated rates of anaerobic microbial processes and can promote organic matter preservation in the sediments (Middelburg and Levin, 2009; Treude, 2011), though a recent study suggests a thin reactive surface layer can provide high rates of organic matter degradation in anoxic environments (Van De Velde et al., 2023). Persistent anoxia in these coastal OMZ can lead to huge releases of sulfide (up to 13.7 mmol m^{-2} d^{-1}) and ammonium (up to 21.2 mmol m^{-2} d^{-1}) into the water column (Sommer et al., 2016).

The Santa Barbara Basin (SBB) is an example of one of these coastal OMZs that experiences seasonal deoxygenation. Drastic changes in water column oxygenation and seafloor redox

conditions drive complex changes in benthic biogeochemistry and microbiology, evidenced most clearly by the development of thick, expansive mats of giant sulfur-oxidizing bacteria (GSOB) on the SBB seafloor (Bernhard et al., 2003; Prokopenko et al., 2006; Valentine et al., 2016; Kuwabara et al., 1999). A 2016 survey of the basin identified a vast GSOB mat spread over 1.6 contiguous km, confined between 487 and 523 km in the SBB depocenter where conditions were anoxic but not depleted of NO_3^- (Valentine et al., 2016). These GSOB mats have been noted previously in the SBB benthos, appearing at times of anoxia and disappearing when oxygen is present in the bottom water (Reimers et al., 1996; Kuwabara et al., 1999). Similar GSOB mats have been identified in other transiently deoxygenated OMZs such as the Peruvian/Chilean coast (Sommer et al., 2016; Schulz et al., 1996; Zopfi et al., 2001; Høgslund et al., 2009). The chemoautotrophic bacteria that constitute the bulk of GSOB mats (typically *Thioploca* and/or *Beggiatoa*) utilize sulfide as an electron donor and O_2 or NO_3^- as a terminal electron acceptor (Jørgensen and Nelson, 2004). Some GSOB can hyperaccumulate NO_3^- in cell vacuoles up to 500 mM (Fossing et al., 1995) and use this NO_3^- reserve to oxidize sulfide that diffuses from the underlying sediment to perform their metabolism. (Huettel et al., 1996; Mußmann et al., 2003; Sayama, 2001).

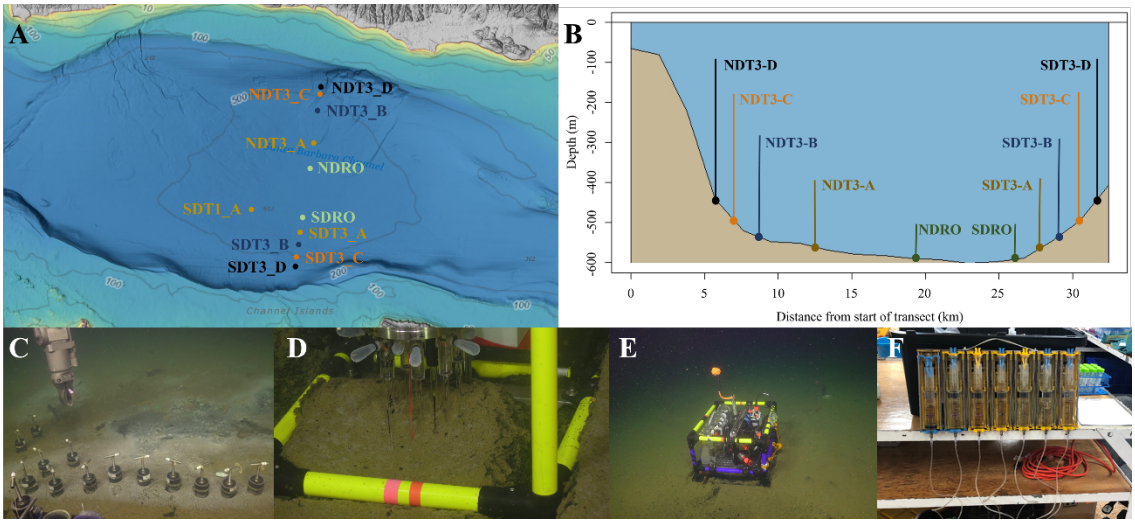

Figure 1. Maps of sampling locations in the Santa Barbara Basin and photographs of deployed equipment: (A) bathymetric map of the Santa Barbara Basin with locations of all sampled stations; (B) cross-section of the Santa Barbara Basin with locations of all sampled station; (C) sediment push coring with ROV arm; (D) sediment microprofiler; (E) benthic flux chamber; (F) closeup of a syringe system from a benthic flux chamber. The map in (A) was generated using the Bathymetric Data Viewer provided by the National Centers for Environmental Information.

The activity of GSOB mats contribute significantly to element cycling in benthic marine environments with large effects on biogeochemical conditions in the bottom water. Isotopic measurements of $^{15}N/^{14}N$ and $^{18}O/^{16}O$ from NO_3^- in the SBB water column suggest that benthic organisms are responsible for approximately 75% of the total NO_3^- reduction in the SBB (Sigman et al., 2003). Other studies found that GSOB mats inhibit the diffusion of NO_3^- into sediments via hyper-accumulation in vacuoles thereby creating conditions ideal for bacterial heterotrophic sulfate reduction beneath them (Fossing et al., 1995; Zopfi et al., 2001). These studies suggest that GSOB mats in the SBB may be responsible for the majority of NO_3^- consumption in the basin rather than water-column microbes. Additionally, GSOB mats have been reported to deplete NO_3^- via dissimilatory nitrate reduction to ammonia (DNRA) in the anoxic bottom water of the Peruvian OMZ (Dale et al., 2016) and in the hypoxic transition zone

106 in the Eastern Gotland Basin of the Baltic Sea (Noffke et al., 2016). By contrast, benthic
107 microbial communities in the hypoxic (42 μM) Mauritanian OMZ perform canonical
108 denitrification instead (Dale et al., 2014). The contrast between the Peruvian and Mauritanian
109 OMZ suggests that bottom- water anoxia triggers the appearance of GSOB mats, and that DNRA
110 is more prevalent where GSOB mats are present.
111
112 The rapid accumulation and consumption of NO_3^- by GSOB mats has ramifications for the redox
113 conditions in the sediment underneath. The depletion of NO_3^- and shallowing of the nitracline
114 could promote high rates of sulfate reduction in the sediment underneath the GSOB mat. In
115 return, the sulfate reduction zone exists close to the sediment-water interface, providing the
116 GSOB mat with readily accessible sulfide. If a metabolic feedback loop is then established
117 between sulfur-oxidizing bacteria at the sediment-water interface and sulfate-reducing bacteria in
118 the sediment, increased NO_3^- loss from the water column and spreading of sulfidic conditions in
119 SBB sediment is expected. With these mats being potentially crucial to nitrogen and sulfur
120 cycling in sediments underlying OMZs, their biogeochemical transformations and ergo effect
121 upon basin redox conditions are critically important to understanding element cycling in the
122 SBB. Such gained knowledge would have additional benefits for predicting biogeochemical
123 feedbacks to the projected expansion of oceanic oxygen deficiency, in the SBB and in OMZs
124 more general, as a result of global change (Stramma et al., 2008).
125
126 Utilizing in-situ technologies, sediment porewater extraction, solid phase analyses, and
127 radiotracer techniques, this study aims to answer the following overarching questions: (1) Which
128 environmental conditions initiate and sustain the proliferation of GSOB mats? (2) Which

129 biogeochemical transformations occur in the sediment underneath these mats? (3) What role do
130 the mats play in the increasingly prevalent anoxic and nitrate-depleted condition found in the
131 SBB? These investigations represent the first basin-wide geochemical characterization of the
132 Santa Barbara Basin which hosts the largest as-of-yet mapped GSOB mat in the world's oceans.
133 It is the first suite of in-situ flux measurements carried out in the SBB, which is unique to other
134 heavily studied marine settings (e.g., Eastern Gotland Basin, Peruvian upwelling zone) in that it
135 is an oceanic basin within an upwelling zone. The results presented here also provide
136 geochemical context for a number of other related investigations in the SBB (Robinson et al.,
137 2022; Xuefeng Peng et al., 2023; Peng et al., 2023) as well as the first measurements in a multi-
138 year study of biogeochemical changes in response to warming waters and increased stratification
139 on the California coast.

2. Materials and Methods

2.1 Study Site

The Santa Barbara Basin (SBB) is a coastal basin in the California Borderland with an approximate maximum depth of 600 m characterized by a seasonally anoxic water column (Sverdrup and Allen, 1939; Sholkovitz and Gieskes, 1971). The transform boundary along the California Borderland heavily affects the geomorphology of basins in this region; these basins become twisted as the plates rub against each other and form a series of "bathtubs" blocked by sills and seamounts off the coast of California. The SBB is bordered by the California coast in the north, the Channel Islands in the south, the Santa Monica basin to the east, and the Arguello Canyon to the west. A sill to the west of the basin at around 475 m depth (Fig. 1) prohibits most water transfer between the Santa Lucia Slope and the deeper waters of the SBB (Sholkovitz and Gieskes, 1971). The highly productive surface waters in the basin provide ample organic matter to the basin's water column, encouraging strong remineralization processes below the euphotic zone, which can induce anoxia below the sill depth, with typically less than 1 μmol O_2 L^{-1} (Sholkovitz, 1973; Emery et al., 1962; Thunell, 1998; Emmer and Thunell, 2000). Benthic faunal distribution within the basin is tightly correlated with this sill depth and related oxygen conditions; below the sill, the sea snail *Alia permodesta* is the most commonly found benthic fauna, while sea stars, sea urchins, and other echinoderms increase in density above the sill (Myhre et al., 2018). During upwelling events (usually in Spring), oxygenated waters from the California Current spill over the western sill and ventilate the SBB, reportedly increase bottom water oxygen concentrations to approximately 20 μmol O_2 L^{-1} (Goericke et al., 2015). SBB water-column oxygen and nitrogen concentrations have been evaluated through a longitudinal survey by the California Cooperative Oceanic Fisheries Investigations (Calcofi) with data

starting in the 1950's . The data collected by this survey shows increasing durations of anoxia and fixed nitrogen loss in the basin with the SBB becoming completely nitrate-depleted below the sill at least three times between 2012 and 2017 (https://calcof.iorg/data/).

2.2 Benthic sediment sampling and instrument deployment

Sediment samples were taken between 30 October and 11 November 2019 during an expedition aboard the research vessel *(R/V) Atlantis* equipped with the remote operated vehicle (ROV) Jason. Samples were taken at stations along a bimodal, north-south transect through the depocenter of the SBB, as well as one station on a separate transect. Details of sampling stations can be seen in Fig. 1A and 1B. Briefly, depocenter stations are labeled as NDRO and SDRO (northern and southern depocenter radial origin, respectively). The remaining stations are named for the cardinal direction (north vs. south) and the transect number (e.g., SDT1-A is on transect 1 while SDT3-A is on transect 3). As station depth decreases, the alpha suffix increases (e.g., NDT3-A is deeper than NDT3-B, etc.).

ROV Jason conducted sediment push coring and deployed automated benthic flux chambers (BFC) and microprofilers at each station. Bottom water oxygen concentration was determined using an Aanderaa 4831 oxygen optode (Aanderaa Instruments, Bergen, Norway) installed on the ROV. Optical modems (Luma 250LP, Hydromea, Renens, Switzerland) installed on the ROV and the BFC and microprofilers were used to transmit deployment settings and start/terminate measurements of the instruments. Multiple push cores (polycarbonate, 30.5 cm length, 6.35 cm inner diameter) per sampling station were retrieved during ROV Jason deployments (Fig. 1C). Replicate cores from each station were transferred to an onboard 6°C cold room upon recovery

aboard the ship and subsampled for either solid phase analyses, porewater geochemistry, or radiotracer experiments.

2.3 Sediment Core Sub-Sampling

Two replicate ROV push cores that were collected near each other at each station were processed under a constant argon flow to protect redox-sensitive species. Cores were sectioned in 1-cm increments up to 10 cm followed by 2-cm increments. Note, sediments from the NDT3-B station were sliced in 2-cm increments. Sediment subsections were transferred into argon-filled 50-mL conical centrifuge tubes. Sediment samples were centrifuged at 2300 x g for 20 minutes. The centrifugate was subsampled unfiltered as fast as possible (to avoid contaminations with oxygen) for porewater analyses. Solid phase cores were sectioned similar to porewater cores and sub-sampled for sediment density, porosity, and organic matter content. A 10 mL cut-off plastic syringe was used to collect 6 mL of sediment into pre-weighed plastic vials (15 mL snap-cap vials) and stored in the dark at 4°C for sediment porosity and density analysis. Two-mL microcentrifuge tubes were filled with sediment from each depth interval and stored at -30°C for sediment organic matter analyses. One ROV push core per station was sub-sampled with a miniaturized push core (length 20 cm, inner diameter 2.6 cm) and taken immediately to the shipboard radioisotope van for radiotracer experiments (see section 2.5).

2.4 Sediment Porewater Geochemistry

Concentrations of porewater sulfide (Cline, 1969), NH_4^+, PO_4^{3-}, and Fe^{2+} (Grasshoff et al., 1999) were determined shipboard with a Shimadzu UV-Spectrophotometer (UV-1800). Detection limits for sulfide, NH_4^+, PO_4^{3-}, and Fe^{2+} were 1 µM. Subsamples (2 mL) for porewater NO_3^- and

209 NO_2^- concentrations were stored in 2-mL plastic vials with an O-ring, frozen shipboard at -30°C
210 and analyzed back at the home laboratory on the same spectrophotometer using the method
211 following (García-Robledo et al., 2014). The detection limit for NO_3^- and NO_2^- was 0.5 µM.
212 Samples for porewater DIC were preserved shipboard with 5 µL saturated HgCl in headspace
213 free glass vials and stored at 4°C for later analysis following (Hall and Aller, 1992). DIC
214 detection limit was 0.1 mM. Total alkalinity was determined shipboard using direct titration of
215 500 µL of pore water with 0.01M Titrisol® HCl (Pavlova et al., 2008). The analysis was
216 calibrated using IAPSO seawater standard, with a precision and detection limit of 0.05 meq L^{-1}.
217 Subsamples (1 mL) for sulfate and chlorinity were stored in 2-mL plastic vials with an O-ring,
218 frozen shipboard at -30°C and later measured in the lab using a Metrohm 761 ion chromatograph
219 with a methodological detection limit of 30 µM (Dale et al., 2015).
220
221 **2.5 Solid Phase Analyses**
222 Porosity/Density samples were collected in pre-weighed plastic vials and dried at 50°C for up to
223 96 hr until the dry weight was stable. Sediment porosity was calculated by taking the difference
224 between wet and dry sediment weight and divided by the volume of the wet sediment. Sediment
225 density was calculated by dividing the wet sediment weight by its volume. Treatment of
226 sediment subsamples for total organic carbon (TOC), total organic nitrogen (TON), and organic
227 carbon isotope composition ($\delta^{13}C$) were modified from (Harris et al., 2001) and sent to the
228 University of California Davis Stable Isotope Facility for analysis using Elemental Analyzer –
229 Isotope Ratio Mass Spectrometry. TOC and TON were calculated based on the sample peak area
230 corrected against a reference material (alfalfa flour). Limit of quantification based on peak area
231 was 100 µg C with an uncertainty of ± 0.2 ‰ for $\delta^{13}C$.

232

233 **2.6 Sulfate Reduction**

234 To determine ex-situ microbial sulfate reduction rates, whole round sub-cores were injected with
235 10 µL carrier-free ^{35}S-Sulfate radiotracer (dissolved in water, 200 kBq, specific activity 37 TBq
236 $mmol^{-1}$) into pre-drilled, silicon-filled holes at 1-cm increments according to (Jørgensen, 1978).
237 These sub-cores were incubated at 6°C in the dark for 6-8 hours. Incubations were stopped by
238 slicing sediment cores in 1-cm increments into 50-mL centrifuge tubes filled with 20-mL zinc
239 acetate (20% w/w) and frozen at -20°C until analysis at the land-based laboratory. Microbial
240 activity in controls was terminated with zinc acetate (20 mL of 20% w/w) before the addition of
241 radiotracer and subsequent freezing. Lab-based analysis of sulfate reduction rates were
242 determined following the cold-chromium distillation procedure (Kallmeyer et al., 2004).

243

244 **2.7 Benthic In-Situ Investigations**

245 Per station, one to three microprofiler (Fig. 1D) and three BFC (Fig. 1E) deployments were
246 carried out by the ROV Jason at the seafloor. Construction, deployment and operation of
247 automated microprofilers and BFCs followed those described in (Treude et al., 2009). The
248 microprofiler deployed in this study represents a modified, miniaturized version of the
249 instrument described in (Gundersen and Jørgensen, 1990) that was constructed specifically for
250 use by ROV. Microprofilers were outfitted with three O_2-microelectrodes (Glud et al., 2000),
251 two pH-microelectrodes (Revsbech and Jørgensen, 1986), two H_2S-microelectrodes
252 (Jeroschewsky et al., 1996), and one conductivity sensor to determine the position of the
253 sediment-water interface relative to the tips of the microelectrodes. Concentrations of oxygen

254 and sulfide, as well as pH were each calculated from microelectrode readings and averaged for
255 the respective sites where replicates existed.
256
257 The BFC consisted of a frame equipped with a cylindrical polycarbonate chamber (inner
258 diameter = 19 cm) with its lower portion sticking out of the frame. The upper side of the
259 chamber was closed by a lid containing a stirrer (Type K/MT 11, K.U.M., Kiel, Germany),
260 oxygen optodes (Type 4330, Aanderaa Data Instruments, Bergen Norway and Hydroflash,
261 Contros/Kongsberg Maritime, Kongsberg, Norway), a conductivity sensor (type 5860, Aanderaa
262 Data Instruments), and a valve. Prior to insertion into the sediments, the chambers were held
263 upside down by the ROV manipulating arms within approximately 10 m of the seafloor and
264 moved back and forth to make sure that water from shallower depth that may have been trapped
265 was replaced by bottom water. Chamber incubations lasted between 240 and 390 minutes. Each
266 BFC was outfitted with a custom-built syringe sampler containing seven syringes that were
267 connected by tubes to sampling ports in the upper wall of the chambers (Fig. 1F): one injection
268 syringe and six sampling syringes that were fired at regular time intervals over the time course of
269 the deployment. The injection syringe contained de-ionized water and the reduction in salinity in
270 the overlaying water after salinity readings stabilized (i.e., full mixing was achieved) 10-30 min
271 after injection was used to determine BFC volumes (Kononets et al., 2021). Samples obtained
272 from the overlaying water of the BFC were examined for the same geochemical constituents as
273 described above (section 2.4). Benthic fluxes of NO_3^-, NH_4^+, PO_4^{3-}, and Fe^{2+} were calculated as
274 follows:
275
276 $$J = \frac{\Delta c}{\Delta t} * \frac{V}{A} \qquad \text{(EQ \# 2)}$$

277

278 Where J is the flux in mmol m^{-2} d^{-1}, ΔC is the concentration change in mmol m^{-3}, Δt is the time
279 interval in d, V is the overlying water volume in m^3, and A is the surface area of the sediment
280 covered by the benthic flux chamber in m^2. An average flux within BFC's was calculated for
281 stations of similar depth. One chamber per site contained $^{15}N\text{-}NO_3^-$ in the injection syringe for in-
282 situ nitrogen cycling experiments. Results are reported from two of these chambers (SDRO and
283 NDT3-D) and all $^{15}N\text{-}NO_3^-$ chambers were excluded from benthic flux calculations (see next
284 section).

285

286 **2.8 In Situ ^{15}N Incubations**

287 Two hundred μmol of ^{15}N-labeled potassium nitrate (99% ^{15}N; Cambridge Isotopes) was injected
288 into the ^{15}N incubation chamber at each site to obtain a final concentration of ~50 – 100 μM ^{15}N-
289 labeled nitrate. Nitrate was amended at this level to prevent its depletion before the last sampling
290 time point (Valentine et al., 2016). Samples for $\delta^{15}N$ analysis were preserved by filling a pre-
291 vacuumed 12-ml exetainer vial with 0.1 ml 7M zinc chloride as a preservative. Another aliquot
292 (~12 ml) of seawater for ammonium isotope analysis (see section 2.7.2) was filtered through 0.2
293 μm syringe filters and stored frozen. Prior to analyzing the samples in 12-ml exetainer vials, 5
294 mL of sample was replaced with ultra-high purity helium to create a headspace. The
295 concentration and $\delta^{15}N$ of dissolved N_2 and N_2O was determined using a Sercon CryoPrep gas
296 concentration system interfaced to a Sercon 20-20 isotope-ratio mass spectrometer (IRMS) at the
297 University of California Davis Stable Isotope Facility.

298

299 **2.9 Ammonium Isotope Analyses**

The production of $^{15}NH_4^+$ in seawater samples was measured using a method adapted from (Zhang et al., 2007) and described previously by (Peng et al., 2016). In brief, NH_4^+ was first oxidized to NO_2^- using hypobromite (BrO^-) and then reduced to N_2O using an acetic acid-azide working solution (Zhang et al., 2007). The $\delta^{15}N$ of the produced N_2O was determined using an Elementar Americas PrecisION continuous flow, multicollector, isotope-ratio mass spectrometer coupled to an automated gas extraction system as described in (Charoenpong et al., 2014). Calibration and correction were performed as described in (Bourbonnais et al., 2017). The measurement precision was ±0.2 ‰ for $\delta^{15}N$. Depending on the in-situ ammonium concentration, the detection limit for total NH_4^+ production rates ranged between 0.006 and 0.0685 mmol m^{-2} d^{-1}.

3. Results

3.1 Bottom water conditions

O_2 and NO_3^- concentrations in the bottom water along the transects can be seen in Table 1. O_2 concentrations below detection as determined by the ROV sensor could in some cases be considered to represent anoxia (0 μM O_2) based on a set of different analytical methods (see discussion section 4.1). Bottom water solute concentrations (as defined by the average T_0 concentration in BFC at each site) can be seen in Suppl. Figs. 1-4. Bottom water NO_3^- concentrations roughly decreased with station depth (e.g., 28 μM at NDT3-D vs. 19 μM at NDRO). Bottom water NO_2^- concentrations were below detection at all stations. Bottom water NH_4^+ concentrations were 9 μM at NDRO and 13 μM at SDRO and below detection in shallower stations. Bottom water PO_4^{3-} concentrations roughly increased with increasing basin depth (e.g., 2 μM at SDT3-D vs. 7 μM at SDRO). Finally, Fe^{2+} was 2 and 5 μM at the NDRO and SDRO stations, respectively and below detection at all shallower stations.

3.2 Sediment characteristics

Photographs of sediment cores with a depth scale are shown below Table 1. Sediment colors were classified according to (Hossain et al., 2014). Cores from the shallowest (D) stations were uniformly reddish in color with small pockets of black. The sediment color changed with station depth, transitioning from a reddish color in the shallowest stations to predominantly black with reddish laminations at the depocenter stations. The band of black sediment appeared at approx. 8 cm sediment depth in the C-station cores and became progressively more ubiquitous with station depth. Notably, NDT3-C sediment (Table 1B) contained black bands from approx. 6-14 cm sediment depth, while SDT3-C sediment (Table 1J) had a much narrower band around 8-10 cm.

Sediment cores from shallower stations (D and C stations) contained signs of bioturbation (e.g., u-shaped burrows) and, in some cases, contained visible macrofauna, such as polychaetas and mollusks. Deeper in the basin (A and depocenter stations) no signs of bioturbation were detected,

Table 1. Station details and photos of representative ROV push cores taken at each station. Mat presence (Y = yes, N = no) was determined visually. Station water depth and oxygen concentration were determined by sensors attached to ROV Jason (bdl = below detection limit (<3 µM O_2). Anoxia was confirmed by additional methods (see discussion section 4.1). Latitude and longitude were determined by triangulation between the ROV and the ship. Bottom water nitrate concentration was derived from an average of benthic flux chamber nitrate measurements at time 0 for each station (chambers with no calculatable flux and ^{15}N-nitrate addition excluded). Note, benthic flux chambers were not deployed at SDT1-A. Photographs show the sediment-water interface (SWI; top part) and each sediment core in full length (lower part).

Parameter	NDT3-D	NDT3-C	NDT3-B	NDT3-A	NDRO	SDRO	SDT1-A	SDT3-A	SDT3-B	SDT3-C	SDT3-D
Mat Present	N	N	N	Y	Y	Y	Y	Y	N	N	N
Depth (m)	447	498	537	572	580	586	573	571	536	494	447
Latitude (°)	34.363	34.353	34.333	34.292	34.262	34.201	34.212	34.184	34.168	34.152	34.142
Longitude (°)	-120.015	-120.016	-120.019	-120.026	-120.031	-120.044	-120.116	-120.047	-120.053	-120.050	-120.052
Oxygen (µM)	8.7	5.2	12.2	9.2	0.0	0.0	0.0	0.0	1.8	3.1	9.6
Nitrate (µM)	27.3	26.0	11.5	24.4	18.5	9.9		20.4	20.6	16.3	28.0

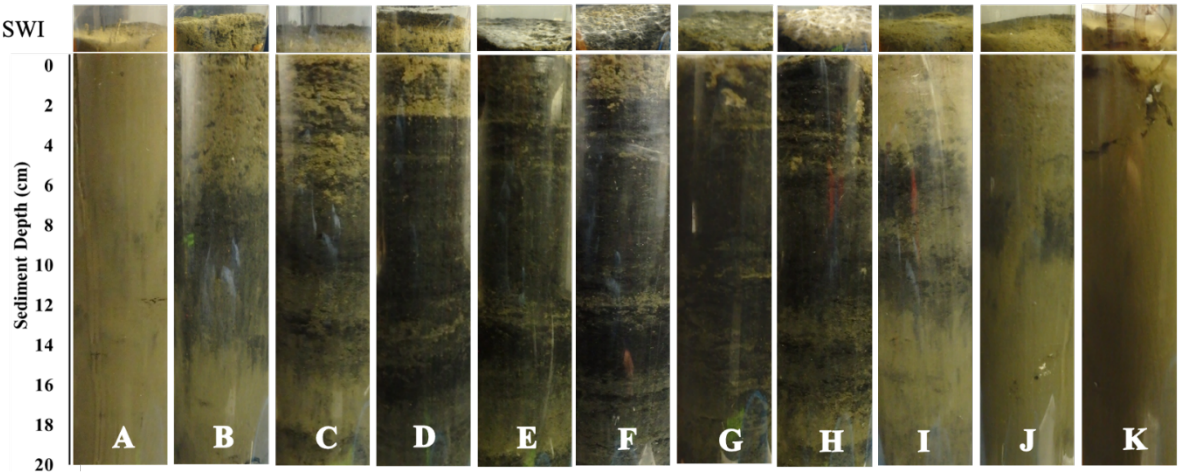

and the sediment-water interface was colonized by patches of white GSOB mats. Spherical cells (given the moniker 'ghost balls') were found mixed amongst giant sulfur bacteria filaments within the top 0-1 cm of sediment at NDRO (Suppl. Fig. 7). These unknown species had similar morphological characteristics to the species *Thiomargarita namibiensis* (Schulz et al., 1999; Schulz and Schulz, 2005) containing a translucent cell with sulfur granules giving them a ghostly

white appearance. A small sample of cells (n = 8) were measured, featuring diameters between 48.0 and 99.6 µm, amounting to an average biovolume of 2.5 x 10^5 µm^3, compared to *T. namibiensis* with a cell diameter usually between 100-300 µm (Schulz et al., 1999).

Table 2. Sediment solid phase data: porosity, density, total organic carbon (TOC), total organic nitrogen (TON), C:N ratio, and δ13C. All data were averaged for the top 0-19 cm sediment, except NDT3-C (17 cm), NDT3-A (11 cm) and SDRO (7 cm), where the core length was shorter. Integrated sulfate reduction rates (iSRR) were integrated over 0-14 cm sediment depth. No sulfate reduction rates are available for NDT3-B, SDT3-A, and SDT3-B; rates were not integrated for SDRO due to missing surface samples.

Parameter	NDT3-D	NDT3-C	NDT3-B	NDT3-A	NDRO	SDRO	SDT1-A	SDT3-A	SDT3-B	SDT3-C	SDT3-D
Porosity	0.79 ± 0.03	0.81 ± 0.04	0.86 ± 0.04	0.88 ± 0.03	0.88 ± 0.04	0.87 ± 0.03	0.88 ± 0.03	0.86 ± 0.04	0.85 ± 0.04	0.82 ± 0.04	0.78 ± 0.04
Density	1.21 ± 0.07	1.16 ± 0.08	1.06 ± 0.08	1.05 ± 0.04	1.06 ± 0.03	1.04 ± 0.03	1.11 ± 0.23	1.05 ± 0.05	1.12 ± 0.06	1.22 ± 0.05	1.22 ± 0.03
TOC (%)	2.9 ± 0.5	2.5 ± 0.5	3.6 ± 0.5	3.1 ± 0.4	3.3 ± 0.4	3.5 ± 0.4	4.5 ± 0.5	3.2 ± 0.0	3.6 ± 0.6	3.6 ± 0.8	3.3 ± 0.5
TON (%)	0.3 ± 0.1	0.5 ± 0.1	0.4 ± 0.1	0.4 ± 0.1	0.4 ± 0.0	0.4 ± 0.1	1.0 ± 0.1	0.4 ± 0.0	0.4 ± 0.1	0.4 ± 0.1	0.4 ± 0.1
C:N Ratio	8.9 ± 0.2	8.7 ± 0.5	8.5 ± 0.5	8.2 ± 0.2	8.2 ± 0.4	8.0 ± 0.2	8.6 ± 0.8	8.3 ± 0.6	8.3 ± 0.3	8.7 ± 0.3	8.5 ± 0.2
δ^{13}C (‰)	-22.4 ± 0.3	-22.4 ± 0.4	-22.2 ± 0.4	-22.1 ± 0.2	-22.1 ± 0.2	-22.0 ± 0.3	-21.3 ± 0.7	-22.1 ± 0.4	-22.0 ± 0.2	-21.9 ± 0.2	-22.0 ± 0.1
Integrated SRR (mmol m^{-2} d^{-2})	2.9	3.8		2.7	4.1		2.9			1.7	1.9

B station cores contained sporadic GSOB filaments slightly deeper in the sediment (approx. 2-4 cm sediment depth). Sediment solid phase parameters (averaged over the entire sediment core depth) can be seen in Table 2. Average sediment porosity increased with basin depth (e.g., from 0.79 at NDT3-D to 0.88 at NDRO). TOC, TON, the C/N ratio, and the δ^{13}C isotopic signature of organic carbon remained relatively constant (2.5 – 4.5%, 0.1 – 0.4%, 8.0 – 8.7 and 21.3 – 22.4 ‰, respectively) over all stations.

3.3 Sediment porewater geochemistry

Total alkalinity (Figs. 2 A-E & 3 A-F) increased steadily with sediment depth at all stations starting with, on average, 2.4 mM in the core supernatant reaching a maximum at the respective deepest sediment sample (20 cm). Porewater alkalinity and DIC also increased with basin depth

(Figs. 2 A-E & 3 A-F) indicating that total alkalinity was dominated by the carbonate system. Porewater DIC was, on average, 2.2 mM in the core supernatant and reached maximum concentrations at the deepest sediment depth (20 cm) at most stations.

Porewater PO_4^{3-} profiles (Figs. 2 A-E & 3 A-F) were markedly different between the depocenter and shallower C and D stations. Porewater PO_4^{3-} concentrations in the depocenter and A stations generally increased with sediment depth but several profiles (NDT3-C, NDT3-A, SDRO, SDT1-A) remained unchanged or decreased deeper in the sediment (starting at approx. 10 cm). The profiles in C and D stations showed a peak in PO_4^{3-} concentrations near the sediment-water interface, particularly in the northern basin. Below 2 cm, PO_4^{3-} decreased with sediment depth, but sometimes showed a second small peak deeper in the sediment (12-14 cm at NDT3-D and 10-12 cm at SDT3-D).

Porewater NH_4^+ concentrations (Figs 2 & 3 A-E) showed trends often similar to alkalinity and DIC; NH_4^+ concentrations increased downcore and were higher at depocenter than at D stations (e.g., 370 and 91 μM at 20 cm for SDRO and SDT3-D, respectively). Porewater NO_2^- (Suppl. Table 1) and NO_3^- (Figs. 2 F-J & F G-L) concentrations were at or near zero below 2 cm at every station, except at SDRO and NDT3-A where large peaks in NO_3^- (376 and 81 μM, respectively) and NO_2^- (37 and 5 μM, respectively) occurred in the top 1 cm.

Porewater Fe^{2+} concentrations (Figs. 2 F-J & 3 G-L) were several orders of magnitude higher at shallower D-stations (max. 722 and 395 μM at NDT3-D and SDT3-D, respectively) compared to depocenter stations (max. 13 and 51 μM at NDRO and SDRO, respectively). NDT3-C porewater

401 Fe^{2+} concentration (Fig. 2G) peaked in the top 1 cm of sediment (similar to deeper stations)
402 while SDT3-C porewater Fe^{2+} concentration (Fig. 3H) peaked around 5-cm sediment depth. Fe^{2+}
403 concentrations reached a max. at 0-2 cm and declined sharply with depth in depocenter and A-
404 station sediment. Northern basin sediment was similar, but the decline in Fe^{2+} below 0-2 cm was
405 less pronounced.
406
407 Maximum porewater sulfide concentrations (Figs. 2 F-J & 3 G-L) were several orders of
408 magnitude lower at the shallower D-stations (5 and 4 μM at NDT3-D and SDT3-D, respectively)
409 compared to A stations (350 and 148 μM at NDT3-A and SDT1-A, respectively). Unlike Fe^{2+},
410 peaks in sulfide concentration occurred deeper in the sediment (e.g., below 5 cm depth at A
411 stations). Porewater sulfate concentrations (Figs. 2 K-O & 3 M-R) decreased slightly with depth,
412 but never reached values below 20 mM at any station.
413
414 **3.4 In-situ microprofiling**
415 Microprofiler O_2 and sulfide measurements are shown in Fig. 4. Oxygen was rapidly consumed
416 within the first 0-1 cm of sediment at every station where O_2 was detected in the bottom water
417 (i.e., at all stations except NDRO, which showed no positive signal of oxygen in the water
418 compared to the sediment; note that no oxygen profile is available for SDRO). Sulfide
419 concentrations from microsensors showed similar trends to spectrophotometric measurements,
420 albeit with different absolute values (below detection in shallower B-, C- and D-stations that
421 lacked mats and >1,000 μM at A- and depocenter stations). Microprofiler pH (Fig. 4) was near
422 7.5 in the bottom water at all stations, and slowly decreased to near 7.0 in the lower parts (3-5

cm) sediment at most stations except NDT3-C and SDT3-B. pH at 2.5 cm at SDT3-B reached 6.77, which was the lowest observed during this expedition.

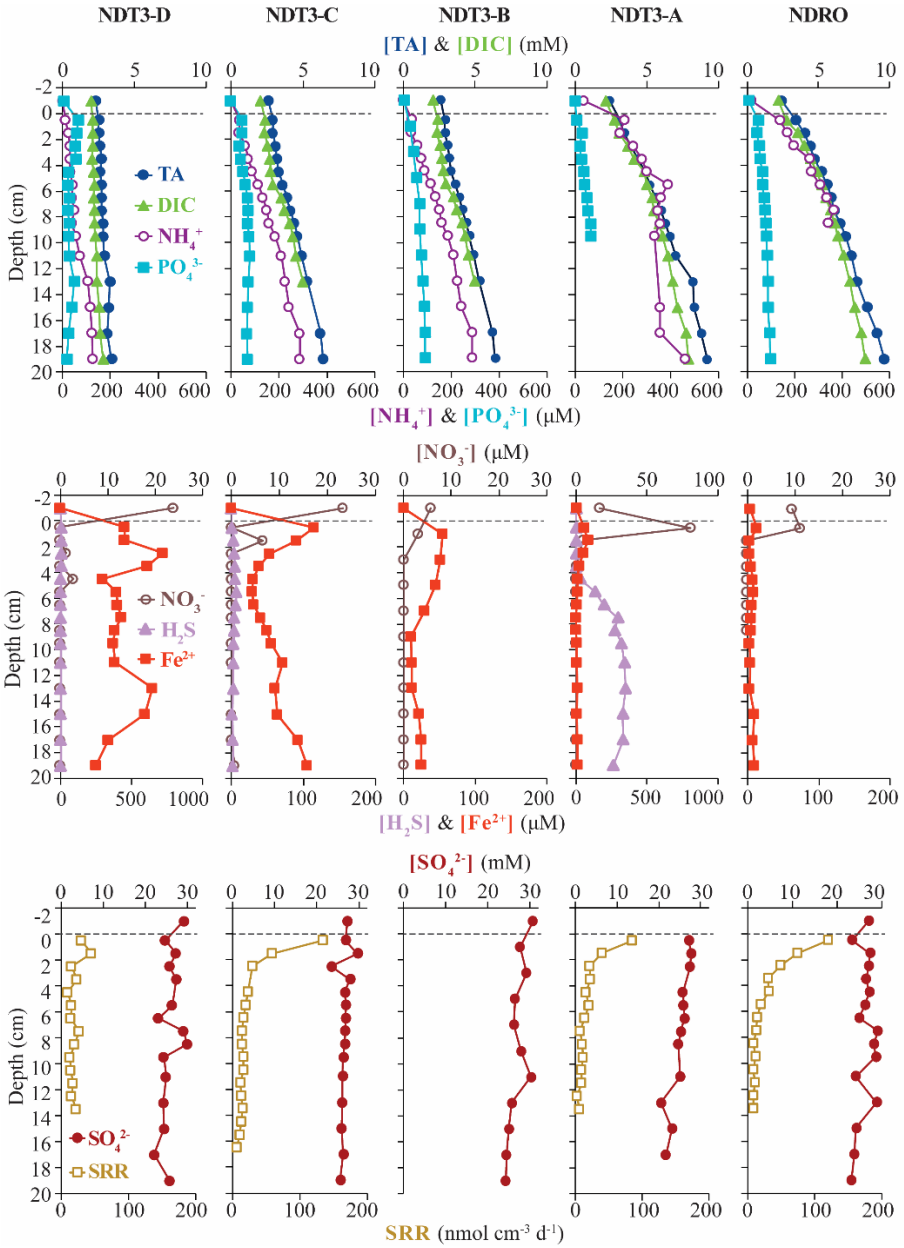

Figure 2. Biogeochemical data from ROV sediment push cores collected at stations on the northern transect (NDT3) and in the northern depocenter (NDRO): total alkalinity (TA), dissolved inorganic carbon (DIC), ammonium (NH_4^+), phosphate (PO_4^{3-}) in the first row; nitrate (NO_3^-), total sulfide (sulfide), and iron (II) (Fe^{2+}) in the second row; sulfate (SO_4^{2-}) and bacterial sulfate reduction rate (SRR) in the third row. Data analyzed from sediment core supernatant are plotted at -1 cm sediment depth; the dotted line connotes the sediment-water interface. Note the change in scale on the primary x-axis in panel I and the change in scale of the secondary x-axis in panels F and I. No spectrophotometric sulfide data is available for NDRO and NDT3-B and no SRR data is available for NDT3-B. For station details see Fig. 1 and Table 1.

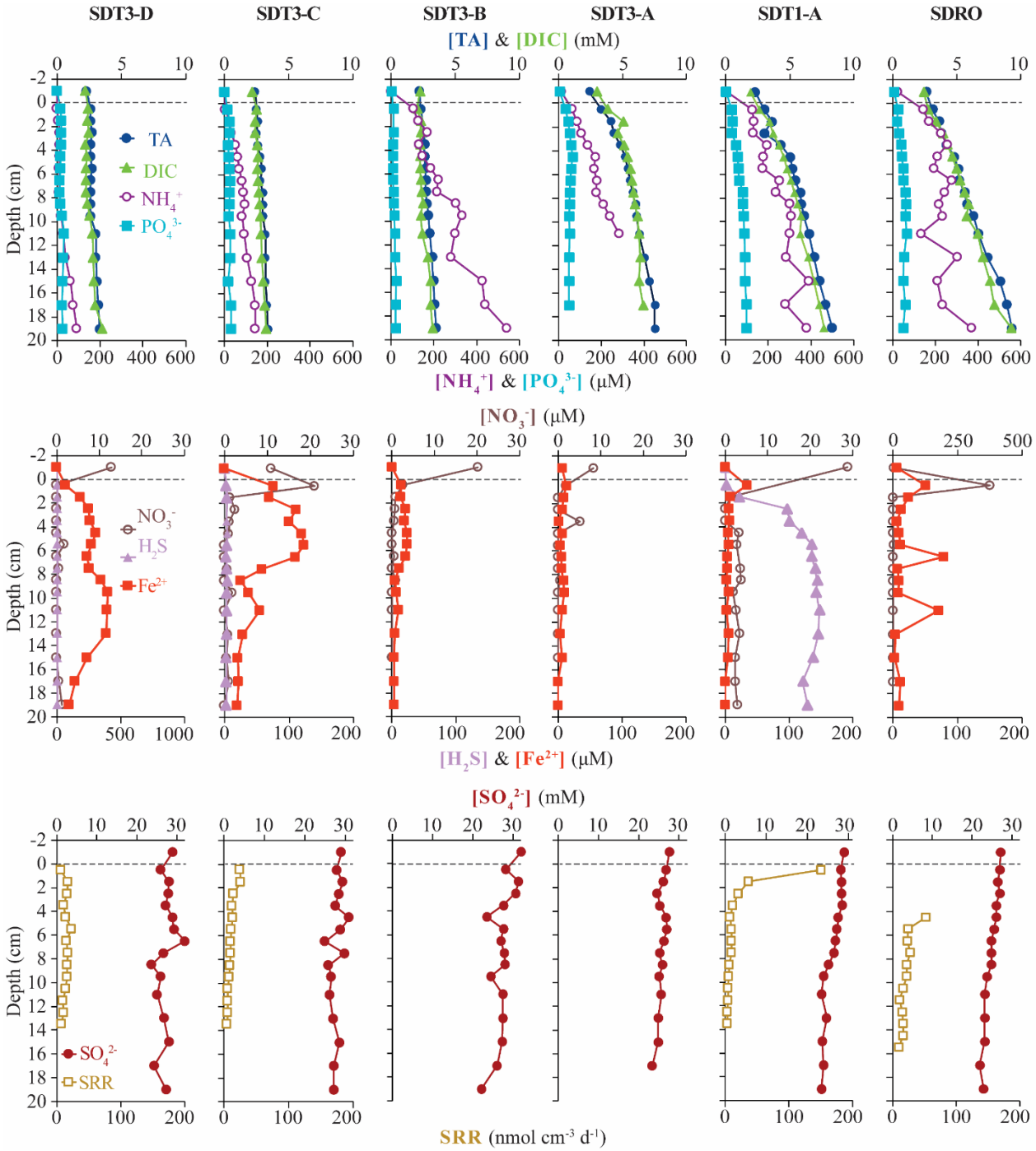

Figure 3. Biogeochemical data from ROV sediment push cores collected at stations on the two southern transects (SDT1 and SDT3) and the southern depocenter (SDRO): total alkalinity (TA), dissolved inorganic carbon (DIC), ammonium (NH_4^+), phosphate (PO_4^{3-}) in the first row; nitrate (NO_3^-), total sulfide (sulfide), and iron (II) (Fe^{2+}) in the second row; sulfate (SO_4^{2-}) and bacterial sulfate reduction rate (SRR) in the third row. Data analyzed from sediment core supernatant are plotted at -1 cm sediment depth; the dotted line connotes the sediment-water interface. Note the change in scale on the primary x-axis in panel L and the change in scale of the secondary x-axis in panel G. No sulfide nor SRR data are available for SDT3-B and -A; spectrophotometric sulfide and the top 0-4 cm of SRR data are not available for SDRO. For station details see Fig. 1 and Table 1.

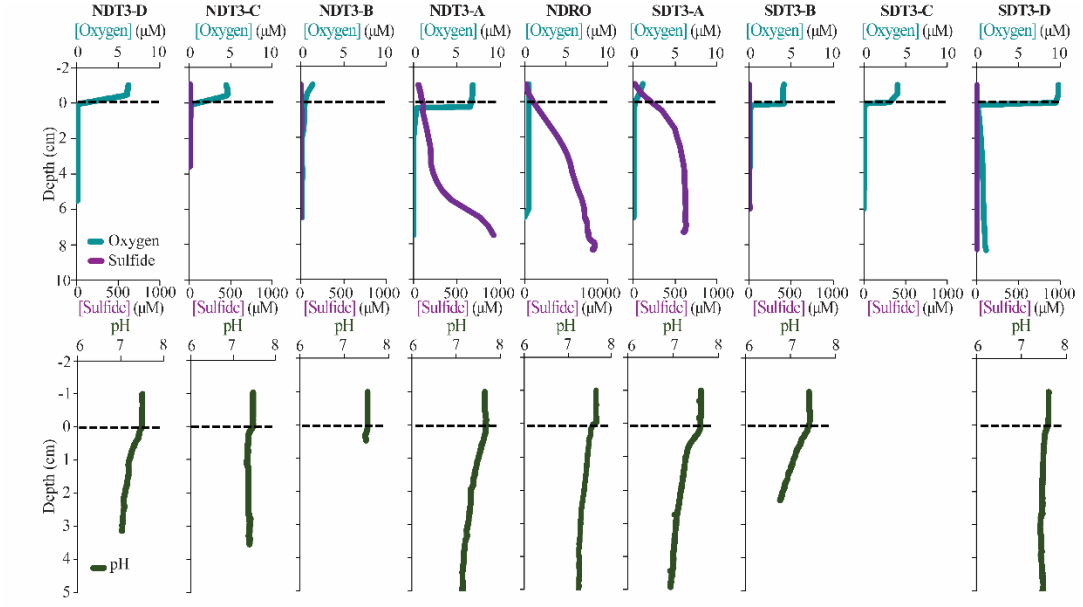

Figure 4. In-situ sediment microprofiler results for all stations (except SDT1-A and SDRO): oxygen (O_2) and total sulfide (sulfide) concentration in the first row; pH profiles in the second row. Note the change in scale on the secondary x-axis for NDRO sulfide. Values determined in the overlying water are plotted at negative sediment depths; the dotted line connotes the sediment-water interface.

3.5 In-situ fluxes of benthic solutes

NO_3^-, NH_4^+, PO_4^{3-}, and Fe^{2+} flux measured in the BFC revealed different patterns of uptake and release from the sediment throughout the basin (Fig. 5 and Suppl. Figs. 1-4). BFC O_2 concentrations were compromised by O_2 release from the chamber's polycarbonate walls, which prevented an accurate calculation of O_2 fluxes from BFC sensor data. NO_3^- was consumed at all stations as indicated by a negative flux (i.e., a flux into the sediment). On the contrary, benthic release (i.e., a flux out of the sediment) was observed for all other analyzed solutes (NH_4^+, PO_4^{3-}, and Fe^{2+}), with the lowest fluxes in the shallow D and C-stations and highest fluxes in the depocenter. Ammonium fluxes were the highest of all the determined solutes and showed the largest difference between deep and shallow stations, with a flux of 1.6 mmol m^{-2} d^{-1} at NDT3-C

(there were no measurable NH_4^+ fluxes in D-station chambers) and reaching 11.1 ± 3.1 mmol m^{-2} d^{-1} (n = 3) at the two depocenter stations. The depocenter ammonium flux far-outpaced the concomitant flux of nitrate into depocenter sediments (-3.2 ± 0.7 mmol m^{-2} d^{-1}, n = 3). Iron and phosphate fluxes were similar at depocenter stations (4.1 ± 0.7, n = 3, and 3.2 ± 0.7, n = 3, mmol m^{-2} d^{-1}, respectively). Alkalinity and DIC concentrations from flux chambers (Suppl. Figs. 5 and 6) remained constant at all stations and thus no DIC flux was calculated. Results from BFCs injected with ^{15}N-NO_3^- at the SDRO and NDT3-D station are shown in Fig. 6. The rates of denitrification, anammox, and N_2O production were higher at SDRO compared to NDT3-D. $^{15}NH_4^+$ production (DNRA) was one order of magnitude higher at the SDRO station (2.67 mmol m^{-2} d^{-1}) compared to the NDT3-D station (0.14 mmol m^{-2} d^{-1}). DNRA accounted for a much higher percentage of NO_3^- reduction at SDRO (54.1%) than NDT3-D (13.3%).

3.6 Sulfate reduction rates

Vertical profiles of bacterial sulfate reduction as determined by the radioisotope technique differed throughout the basin (Figs. 2 & 3). Peaks in sulfate reduction were seen in the top 0-1 cm of sediment at stations with a visible GSOB mat on the surface (120.2, 151.0, and 85.3 nmol cm^{-3} d^{-1} at NDRO, SDT1-A, and NDT3-A, respectively). Sediments at most shallower basin depths exhibited peaks slightly deeper in the sediment and of lower magnitude (25.5, 44.5, 22.5 nmol cm^{-3} d^{-1} at SDT3-C, NDT3-D, and SDT3-D respectively). NDT3-C had no visible GSOB mats but exhibited a peak (133.7 nmol cm^{-3} d^{-1}) in sulfate reduction at 0-1 cm depth, similar to deeper stations (e.g., NDRO in Fig. 2O), which differed from other shallow stations (e.g., SDT3-C in Fig. 3N). The integrated sulfate reduction rate (0-14 cm depth) at NDRO (4.1 mmol m^{-2} d^{-1}) was noticeably higher than most other stations with the exception of NDT3-C (3.8 mmol m^{-2} d^{-1})

488 (Table 2). NDT3-D and NDT3-C exhibited higher integrated rates (2.9 and 3.8 mmol m^{-2} d^{-1})
489 than their southern station counterparts SDT3-D and SDT3-C (1.9 and 1.7 mmol m^{-2} d^{-1}).
490

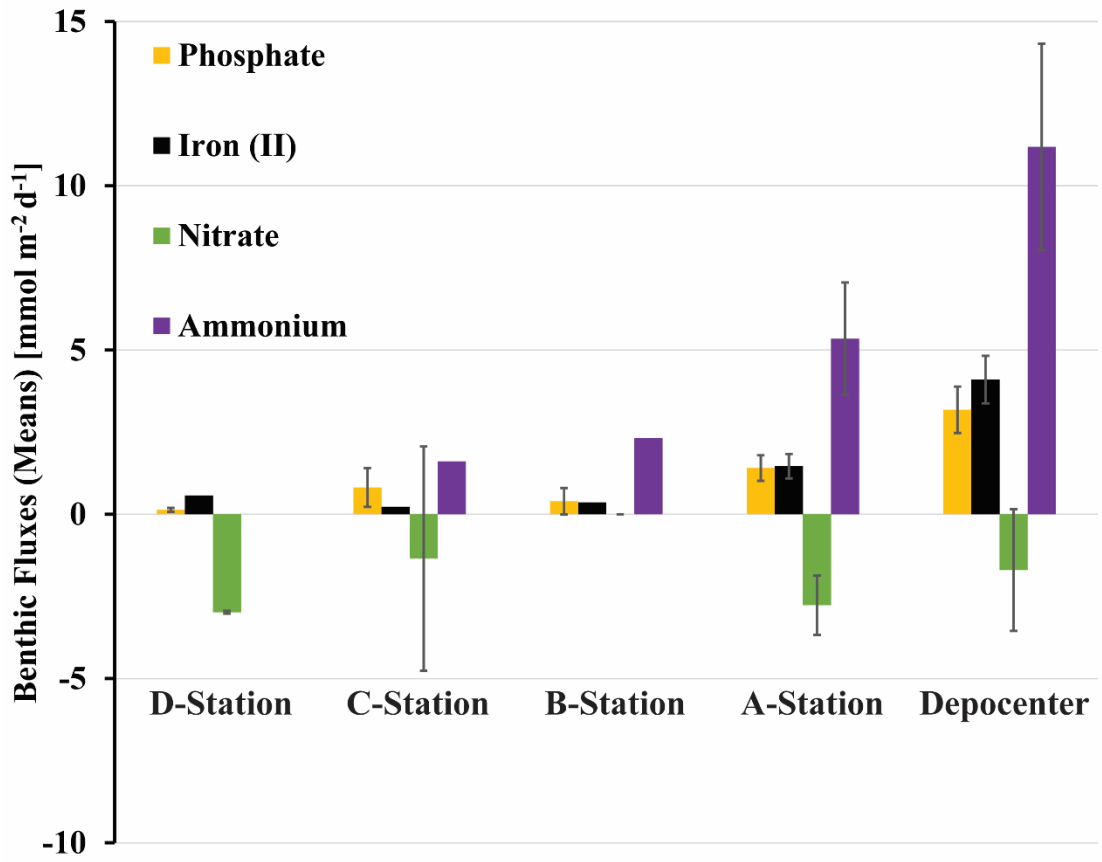

491
492
493 **Figure 5.** Benthic fluxes of solutes (positive flux = release from the seafloor; negative flux = uptake by the
494 seafloor) determined with in-situ benthic flux chambers. Rates were averaged for stations of same depth from
495 the northern and southern transect and the depocenter (NDRO and SDRO). Note, giant sulfur-oxidizing bacterial
496 mats were found at depocenter and A-stations. Error bars represent standard errors.
497

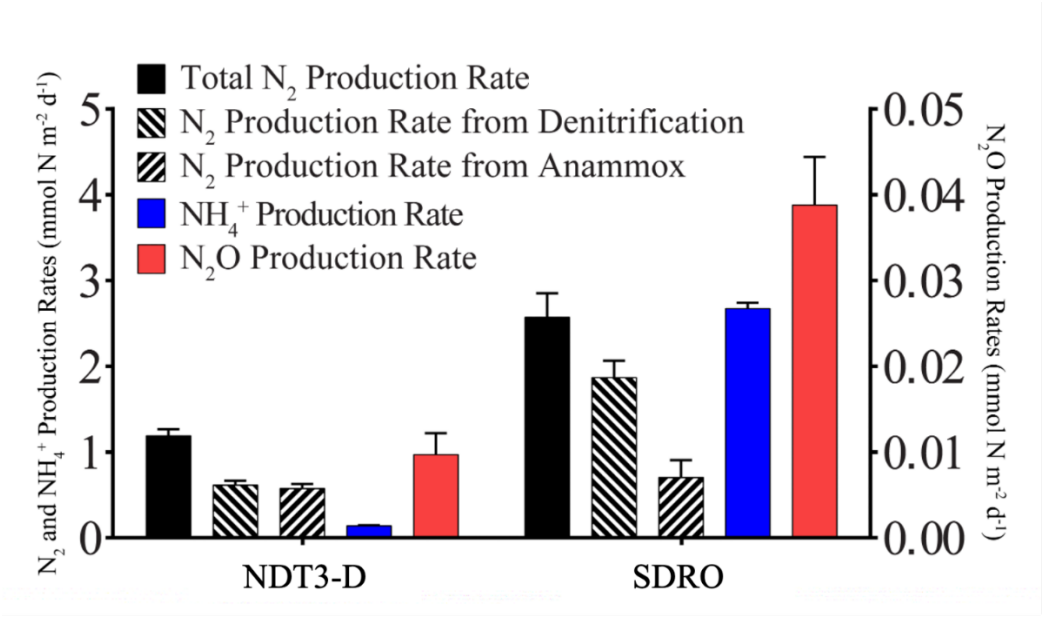

Figure 6. Areal rates of total N_2 production, denitrification, anammox, NH_4^+ production (DNRA), and N_2O production

4. Discussion

4.1 Giant sulfur-oxidizing bacterial mats proliferated in response to deoxygenation in the Santa Barbara Basin

The SBB is an ideal environment to study the effect of transient deoxygenation on benthic biogeochemistry. In Fall 2019, when this expedition took place, the SBB was undergoing a transition from oxygenated to virtually anoxic conditions (Qin et al., 2022). When the AT42-19 cruise occurred, most of the bottom water in the basin was hypoxic (A-, B-, C-, and D-stations), except for the depositional center. Separate O_2 measurements from the ROV sensor (O_2 below detection limit, Table 1), microprofilers (no signal change between water column and sediment, Fig. 4), and Winkler titration from CTD/rosette casts (uniform non-zero value below 500 m (Qin et al., 2022)) indicated full anoxia in the bottom water at the deeper stations (NDRO and SDRO). Notably, bottom water conditions revealed a slight asymmetry between the basin transects (Fig. 1); bottom water along the northern transect generally had more O_2 and NO_3^- than the southern transect (e.g., 9 μM O_2 at NDT3-A and 0 μM O_2 at SDT3-A). This asymmetry indicated differences in the circulation and/or microbial communities between the northern and southern portions of the basin. Whether this asymmetry is a permanent feature of the basin or symptomatic of the specific conditions in November 2019 is unclear; previous studies in the SBB have been restricted to the depocenter or one side of the basin (Sholkovitz, 1973; Reimers et al., 1996; Kuwabara et al., 1999). Regardless of bottom water oxidant concentration, the energetically most favorable terminal electron acceptors (O_2 and NO_3^-) disappeared in a very narrow zone below the sediment-water interface (Fig. 4 and Figs. 2 and 3, respectively), consistent with their expected rapid consumption by the benthic microbial community.

In the present study, benthic GSOB mats were primarily limited to the anoxic depocenter of the SBB. Similarly, such mats were replete in the core of the anoxic Peruvian OMZ (Levin et al., 2002; Sommer et al., 2016; Mosch et al., 2012), but absent from the seafloor below the hypoxic, i.e., slightly oxygenated, Mauritanian OMZ (Schroller-Lomnitz et al., 2019). GSOB mats in November 2019 were observed deeper in the basin than in October 2013 (Valentine et al., 2016) but in a similar location to June 1988 (Reimers et al., 1996) and April 1997 (Kuwabara et al., 1999). During the 2013 sampling, dense GSOB mats were confined to depths between approx. 500-570 m (equivalent to the B-stations from this expedition), corresponding with anoxic conditions in the bottom water. This habitat was sandwiched between an anoxic, anitric (i.e., nitrate-free) deep and a hypoxic, nitrigenated (i.e., nitrate-rich) shallower water layer (Valentine et al., 2016). The difference in depth distribution of GSOB mats between the 2013 and 2019 expedition provides evidence that GSOB mats in the SBB are ephemeral and proliferate where the bottom water is anoxic but not anitric.

As our study represents only a snapshot of an oxygen- and nitrate-driven mat dynamic, we can only speculate how areas of the basin that did not contain GSOB mats in November 2019 fit into this dynamic. For example, mat-forming sulfur bacteria found slightly deeper in the sediment at B-stations (see section 3.2) could be progenitors to surface sediment colonization of thick GSOB mats, as has been recorded in other transiently deoxygenated environments (Jørgensen, 1977). Alternatively, these subsurface colonies could also be remnants of a former surface GSOB mat that retreated under changing redox conditions. Oxygenated conditions in the water preceding the 2019 expedition would, in this context, suggest the mats migrated following a previous anoxic event (Qin et al., 2022). If deoxygenation persisted in the SBB after the AT42-19 cruise,

550 then anitria (i.e., anitric conditions – similar to anoxia) would likely follow in the deepest basin
551 water. These conditions would be similar to those seen in 2013 (Valentine et al., 2016), where
552 GSOB mats formed a contiguous "donut ring" at shallower basin depths. Interestingly, GSOB
553 mats in the Eastern Gotland Basin of the Baltic Sea were confined to a hypoxic transition zone,
554 where O_2 was < 30 μM but did not reach anoxia, while no mats were observed at deeper anoxic
555 locations (Noffke et al., 2016). This difference in distribution compared to the SBB suggests that
556 GSOB mats proliferate under different conditions (anoxic or hypoxic), potentially depending on
557 the species of mat-forming bacteria present and whether they specialize in aerobic or anaerobic
558 chemosynthesis.
559
560 **4.2 Shift from benthic denitrification to dissimilatory nitrate reduction to ammonium in**
561 **response to complete deoxygenation in the Santa Barbara Basin**
562
563 Benthic uptake and release of nitrogen species by SBB sediment appeared to be affected by the
564 presence of GSOB mats. While total benthic nitrate uptake was similar between D- and
565 depocenter stations based on in-situ NO_3^- flux measurements (Fig. 4), NH_4^+ release from the
566 sediment into the water column increased where GSOB mats were present (Fig. 5). This trend is
567 supported by the porewater profiles of NH_4^+, which showed a steeper increase over sediment
568 depth at deeper stations (Figs. 2 & 3). Incubations with ^{15}N-NO_3^- revealed that N_2 production
569 (denitrification and anammox) accounted for 86% of NO_3^-/NO_2^- reduction in the shallow basin,
570 while NH_4^+ production (DNRA) accounted for 13% and N_2O production accounted for 1%
571 (NDT3-D, Fig. 6;(Peng et al., 2023)). In contrast, most (54%) of NO_3^- reduction at the
572 depositional center occurred via DNRA; N_2 production accounted for 45% and N_2O production

accounted for 1% of NO_3^- reduction at the SDRO (Fig. 6; Peng et al. 2023). It is important to note that these results only describe patterns of NO_3^- reduction in the basin, while other mechanisms of nitrate uptake by sediment (e.g., hyper-accumulation of nitrate into vacuoles) are more difficult to calculate accurately.

It is likely important to SBB benthic nitrogen cycling that some eukaryotic organisms can hyper-accumulate NO_3^- in benthic, anoxic environments including diatoms (Kamp et al., 2011) and foraminifera (Risgaard-Petersen et al., 2006). Additionally, meiofauna (e.g., nematodes) can enhance rates of denitrification (Bonaglia et al., 2014). Both foraminifera and meiofauna were observed in SBB depocenter and A-station sediments in November 2019, and diatoms were observed in shallower sediments in the basin (data not shown). Other studies found that benthic foraminifera in the SBB depocenter can hyperaccumulate NO_3^- intracellularly up to 375 ± 174 mM (Bernhard et al., 2012) and host symbionts capable of performing denitrification (Bernhard et al., 2000). These foraminifera were found to be responsible for approx. 3 mM N m^{-2} d^{-1}, or 67% of the total denitrification occurring in the SBB depocenter (Bernhard et al., 2012). Additionally, fungi could reduce NO_3^- or NO_2^- to nitrous oxide in marine sediments and may contribute to denitrification in SBB sediments (Kamp et al., 2015; Lazo-Murphy et al., 2022). This opens up the possibility that the majority of denitrification we observed in the SBB depocenter is performed by eukaryotes, while prokaryotes (especially GSOB) are responsible for most of the DNRA. Elevated NO_3^- and NO_2^- concentrations that were observed in our 0-1 cm samples from NDT3-A and SDRO have been reported from SBB depocenter sediments in the past (Reimers et al., 1996; Bernhard et al., 2003), and have been attributed to both GSOB and benthic eukaryotes. The impact of eukaryotes on SBB benthic nitrogen transformation remains to be disentangled from the mats themselves.

Our data suggests a transition from denitrification-dominated sediment in the oxygenated basin to an increasing influence of DNRA on N cycling in the deeper, anoxic basin. Placed in the context of other OMZs, Mauritanian shelf sediment was dominated by denitrification (Dale et al., 2014), similar to SBB shallow sediment (below hypoxic water) while core Peruvian OMZ sediment was dominated by DNRA, similar to sediment of the deeper SBB (below anoxic water) (Sommer et al., 2016). Nitrate reduction in sediment below the seasonally hypoxic Eckernförde Bay (Dale et al., 2011) and below the hypoxic transition zone of the Eastern Gotland Basin (Noffke et al., 2016) also showed increased DNRA where GSOB mats were present, though with an order of magnitude lower NH_4^+ flux (avg. 1.74 mmol m^{-2} d^{-1} and max. 1.10 mmol m^{-2} d^{-1}, respectively) than the SBB depocenter.

While our study suggests a shift from denitrification to DNRA during deoxygenation of SBB bottom water, other studies examined changes in benthic nitrogen cycling under reverse conditions, i.e., the reoxidation of the environment following anoxia (Hylén et al., 2022; De Brabandere et al., 2015). After a decadal oxygenation event in the Eastern Gotland Basin (Baltic Sea) in 2015-2016, sediment exhibited a slight increase in denitrification, but remained dominated by DNRA and N_2O production (Hylén et al., 2022). The lack of N_2 production via denitrification following this oxygenation event was attributed to the reoxygenation event being too weak to substantially oxidize sediments, which would favor denitrification (Hylén et al., 2022). In an engineered reoxygenation event of the By Fjord on Sweden's western coast, where dissolved O_2 and NO_3^- content of anoxic and anitric bottom water was artificially increased to

approx. 130 μM O_2 and 20 μM NO_3^- over a period of roughly 2 years, denitrification rates were increased by an order of magnitude and DNRA rates were also stimulated (De Brabandere et al., 2015). Comparing our results to these two studies suggests that DNRA bacteria are more resilient to weak reoxygenation events and thrive in transiently deoxygenated systems that remain hypoxic (O_2 < 63 μM). The frequency and magnitude of reoxygenation and deoxygenation of SBB bottom waters, and the effect of these processes on the benthic microbial community, could be a major factor supporting some of the highest recorded total nitrate reduction rates in a natural benthic marine setting (Peng et al., 2023).

Table 3. Example reactions of nitrate reduction pathways with associated energy yield in respect to the electron donor (H_2 or HS^-) and electron acceptor (NO_3^-) and electron accepting capacity. Modified from Table 2 in (Tiedje et al., 1983).

Reaction	$\Delta G^{o\prime}$ (kcal mol^{-1})		Electrons per NO_3^-
	H_2 / HS^-	NO_3^-	
Chemoheterotrophic Denitrification			
$2NO_3^- + 5H_2 + 2H^+ \rightarrow N_2 + 6H_2O$	-53.6	-133.9	5
Chemoautotrophic Denitrification			
$8NO_3^- + 5HS^- + 3H^+ \rightarrow 5SO_4^{2-} + 4N_2 + 4H_2O$	-177.9	-111.2	5
Chemoheterotrophic DNRA			
$NO_3^- + 4H_2 + 2H^+ \rightarrow NH_4^+ + 3H_2O$	-35.8	-143.3	8
Chemoautotrophic DNRA			
$NO_3^- + HS^- + H^+ + H_2O \rightarrow NH_4^+ + SO_4^{2-}$	-107.0	-107.0	8

A high ratio of electron donor to electron acceptor favors DNRA over denitrification (Marchant et al., 2014; Hardison et al., 2015; Tiedje et al., 1983) and this ratio appears to be critical in determining the dominant nitrate reduction pathway in SBB sediments, similar to the Eastern Gotland Basin (Hylén et al., 2022) and the By Fjord (De Brabandere et al., 2015). Example energy yields for denitrification and DNRA are shown in Table 3. As discussed in (Tiedje et al., 1983), heterotrophic denitrification yields more energy per mol of electron donor than DNRA. However, the reverse is true when considering energy yield per mol of electron acceptor (NO_3^-).

DNRA also yields 3 more electrons per molecule of NO_3^- than denitrification. Tiedje et al. argued that in environments that are starved of powerful terminal electron acceptors, such as anoxic, organic-rich sediment, the energy yield per electron acceptor and additional electrons available for transfer could push nitrate reduction towards DNRA. Multiple laboratory and model studies have converged on an electron donor to acceptor ratio of approximately 3 to encourage DNRA over denitrification (Hardison et al., 2015; Algar and Vallino, 2014) though other studies have found higher values (Porubsky et al., 2009; Kraft et al., 2014). Sulfide concentrations near the sediment-water interface at the SBB depocenter (approx. 200 μM at 0.5 cm depth; Fig. 3, NDRO) would favor chemoautotrophic DNRA over denitrification at ambient marine nitrate concentrations (approx. 28 μM). Additionally, DNRA appears to be the preferred nitrate reduction pathway for chemoautotrophs that utilize iron or sulfide as an electron donor (Caffrey et al., 2019; Kessler et al., 2019; An and Gardner, 2002). As GSOB mats hyper-accumulate nitrate from the bottom water into their intracellular vacuoles, the resulting decline in electron acceptors at the sediment-water interface coupled with an elevation of the sulfate reduction zone would create an electron donor to acceptor ratio that favors DNRA. Since GSOB mats in the SBB seem to prefer DNRA, starving the bottom water of electron acceptors coupled with the high sulfate reduction rates could give them a competitive advantage and allow them to proliferate into the largest-yet mapped GSOB mat in Earth's oceans, as seen in other expeditions (Valentine et al., 2016; Reimers et al., 1996; Kuwabara et al., 1999).

4.3 Microbial mat proliferation and benthic phosphate remineralization dependent on high rates of organic matter degradation in the Santa Barbara Basin

663 Organic carbon content of the benthic environment appears to be a key control on sulfate
664 reduction rates near the sediment-water interface as well as microbial mat proliferation. Sulfate
665 reduction rates in the SBB depocenter are most similar in magnitude and profile (i.e., highest
666 rates found at the sediment-water interface and decline drastically thereafter) to those found in
667 sediments below the transiently deoxygenated portion of the Peruvian shelf (e.g., 4.1 mmol m^{-2}
668 d^{-1} at the SBB NDRO station vs. 2.5-3.8 mmol m^{-2} d^{-1} at 128-144 m water depth on the Peruvian
669 margin (Gier et al., 2016; Treude et al., 2021)). The TOC content of surface sediments in these
670 two regions are both high and within the same order of magnitude (maximum recorded TOC of
671 5.2% at the 0-1 cm margin at the SDT1-A station compared with 7.6% in the Peruvian margin
672 145 m depth (Noffke et al., 2012)). In comparison, sulfate reduction rates in the SBB were at
673 least one order of magnitude lower than found in sediment below the OMZ on the Namibian
674 Shelf, which has much higher TOC contents of >10% (Brüchert et al., 2003; Bremner, 1981).
675 Sulfate reduction rates in the shelf sediments below the Eastern Arabian OMZ were much lower
676 (0.18 – 1.27 mmol m^{-2} d^{-1}) than rates in the SBB depocenter (Naik et al., 2017) despite similar
677 hypoxic to anoxic bottom water conditions. These lower sulfate reduction rates were attributed to
678 the relatively low amount of pelagic primary productivity and ergo benthic organic matter
679 delivery in the Eastern Arabian OMZ compared to other upwelling systems (Naik et al., 2017).
680 The organic matter content of the sediment appears to be important in the proliferation of GSOB
681 mats; too much TOC could result in toxic levels of sulfide at the sediment-water interface
682 (*Beggiatoa* exhibit an aversion to sulfidic sediments but toxicity has not been quantified)
683 (Preisler et al., 2007), whereas too little sulfide would not provide enough electron donor for the
684 GSOB's chemoautotrophic metabolism.
685

686 The profiles of several indicators for benthic anaerobic organic matter remineralization (total
687 alkalinity, DIC, PO_4^{3-}, NH_4^+) increased in steepness with increasing water depth (Figs. 2 A-E &
688 3A-F). One divergence from this trend can be seen in PO_4^{3-} profiles from the shallow C- and D-
689 stations, which also featured low rates of sulfate reduction. PO_4^{3-} profiles in these sediments
690 track closely to Fe^{2+} profiles; both solutes dip in concentration in areas with visible iron sulfide
691 formation (e.g., 5-11 cm in NDT3-D as seen in Fig. 2A). Additionally, several stations that
692 exhibited high sulfate reduction rates in surface sediment (e.g., SDT1-A) showed almost no
693 change in PO_4^{3-} at depths below 5 cm (e.g., Fig. 2 K-O compared to Fig. 2 A-E). This
694 phenomenon has been previously documented in SBB sediment and is attributed to the
695 precipitation of carbonate fluorapatite (Reimers et al., 1996). The confinement of these flat PO_4^{3-}
696 profiles to stations with >100 nmol cm^{-3} d^{-1} sulfate reduction in surface sediment suggests that
697 this mineralogical sink of PO_4^{3-} in SBB sediment may be dependent on high sulfate reduction
698 rates, owing to the bicarbonate produced by sulfate reduction (Reimers et al., 1996), and is not
699 found throughout the basin. Flat PO_4^{3-} profiles were also reported from the transiently
700 deoxygenated portion of the Peruvian OMZ, where phosphate mineral precipitation has been
701 documented (Noffke et al., 2012). Similar to the shallow margins of the SBB, PO_4^{3-} in
702 Mauritanian OMZ porewater tracks closely with changes in porewater Fe^{2+} (Schroller-Lomnitz
703 et al., 2019), indicating that iron mineralization/dissolution mechanisms hold a greater influence
704 on PO_4^{3-} concentrations under hypoxic bottom waters.
705
706 **4.4 Iron oxide exhaustion is critical for raising the sulfate reduction zone close to the**
707 **sediment-water interface in Santa Barbara Basin sediment.**
708

709 The hyper-accumulation of NO_3^- by GSOB mats potentially facilitates sulfate reduction close to
710 the sediment-water interface in the SBB (e.g., NDRO and NDT3-A as seen in fig. 2N and 2O) by
711 starving the sediment of this more powerful electron acceptor. The rise of the sulfate reduction
712 zone at NDT3-C (fig. 2L) further suggests that the exhaustion of iron oxides and the formation of
713 iron sulfide below the sediment-water interface may play a crucial role in controlling the
714 distribution of sulfate reduction as well. SBB sediments showed a wide vertical and horizontal
715 heterogeneity of redox states based on visual appearance (Fig. 1A-K). Sediment beneath the
716 hypoxic bottom water at the shallowest D-stations was reddish, consistent with a high content of
717 iron oxides. Interestingly, porewater Fe^{2+} concentrations in shallower parts of the basin (e.g.,
718 NDT3-D, max. ~700 µM Fe^{2+}) were an order of magnitude larger than those found in both the
719 Peruvian (max ~60 and ~30 µM Fe^{2+}, respectively; (Noffke et al., 2012; Plass et al., 2020) and
720 Mauritanian (max. ~50 µM Fe^{2+}; Schroller-Lomnitz et al 2019) OMZ. It should be noted that
721 porewater samples for geochemical analyses were unfiltered and hence reported iron
722 concentrations include aqueous, colloidal, and nanoparticulate species. Regardless, all these
723 components represent bioavailable sources of iron. Further, since filtering through 0.45 or 0.2
724 µm filters only removes a fraction of colloidal particles and no nanoparticles (Raiswell and
725 Canfield, 2012), potential surplus porewater iron in SBB samples in comparison to studies that
726 applied filtering was likely minimal.
727
728 Deeper in the basin, bands of black sediment that appear mid-core at NDT3-C (6-14 cm) and
729 SDT3-C (6-10 cm) indicate the formation of iron sulfides as a result of sulfide produced by
730 sulfate reduction (Canfield, 1989). Both D-stations had similar bottom water conditions (Table
731 1), sulfate reduction rates (Fig. 3W-AG), porewater concentrations of solutes (Figs. 2 and 3), and

732 visual sediment characteristics (Section 3.1). On the contrary, there are some noticeable
733 differences in the porewater geochemistry between the two C-stations. At the C-stations, peaks
734 in sulfate reduction were in the surface sediment, above the iron sulfide layers, and declined
735 below approximately 4 cm, indicating a discrepancy between observed peak sulfate reduction
736 activity and the mineralogical clues left behind by the process. Comparing NDT3-C and SDT3-
737 C, iron sulfide formation (Table 1B compared to 1J), porewater Fe^{2+} profiles (Fig. 2G compared
738 to Fig. 3H), and sulfate reduction rates (Fig. 2L compared to Fig. 3N) show that NDT3-C
739 sediment appears to be in transition towards a more sulfidic state, while SDT3-C sediments still
740 mimic the shallow D-station ferruginous state. While sulfate reduction rates for B-stations are
741 not available due to technical issues during sample processing, porewater Fe^{2+} profiles show a
742 similar difference between the north and south basin (Fig. 2H compared to Fig. 3I) as did visual
743 sediment characteristics (Table 1C compared to 1I). This difference in biogeochemical profiles
744 and apparent minerology between the north and south C- and B-stations could be a result of
745 hydrographic and/or bathymetric differences in the basin (Sholkovitz and Gieskes, 1971; Bograd
746 et al., 2002), but a discernable link between the differences in sediment biogeochemistry and the
747 differences in bottom water oxygen (Table 1) need to be further explored.
748
749 Deeper in the basin (depocenter and A-stations), porewater Fe^{2+} concentrations in sediment
750 beneath anoxic bottom water (max. 84 μM Fe^{2+}) were similar to concentrations found below the
751 Peruvian OMZ in 2008 under anoxic bottom water conditions (78 m water depth, max. 80 μM
752 Fe^{2+}) (Noffke et al., 2012). These deep basin porewater Fe^{2+} concentrations were, however, an
753 order of magnitude larger than those found at a similar site on the Peruvian shelf (75 m water
754 depth, max. 1 μM Fe^{2+}) in 2017 during a kelvin-wave-associated "Coastal El Niño" event that

created oxygenated bottom waters during the sampling and the disappearance of previously observed dense GSOB mats (Plass et al., 2020). As the SBB water column was undergoing rapid deoxygenation in the weeks preceding this study (Qin et al., 2022), the sediments below the sill appeared to be actively shifting from a ferruginous state to a sulfidic state, with this change starting around the C-stations and being complete in the depocenter. Comparing apparent iron sulfide formation with dips in porewater Fe^{2+} concentrations in C-station profiles (Fig. 1B compared to Fig. 2G and Fig. 1J compared to Fig. 3H) signals a shift away from a ferruginous state occurring just below the SBB sill.

C-station porewater Fe^{2+} concentrations and sulfate reduction rates indicate that migration of the sulfate reduction zone towards the sediment-water interface is associated with iron sulfide formation deeper in the sediment. The activity (or lack thereof) of cable bacteria, which are able to bridge the gap between the oxidized sediment-water interface and reduced sediment below using a biofilament (Pfeffer et al., 2012), could explain the interplay between sulfate reduction and iron cycling in SBB sediments. Cable bacteria, such as *Ca. Electronema* sp., contain genes involved in DNRA (Kjeldsen et al., 2019) and can perform nitrate reduction in incubation experiments (Marzocchi et al., 2014), but their direct transformation of NO_3^- in the environment appears limited (Kessler et al., 2019) and they appear to be inactive in anoxic aquatic environments (Seitaj et al., 2015; Marzocchi et al., 2018; Hermans et al., 2019). Cable bacteria primarily conduct aerobic sulfide oxidation (Pfeffer et al., 2012), though they can also utilize Fe^{2+} as an electron donor (Seitaj et al., 2015). The maximum recorded filament length of cable bacteria is 7 cm (Van De Velde et al., 2016), though typically they are not stretched completely vertically through the sediment. The appearance of black sediment in the SBB C-station

778 sediments, starting at approx. 5 cm depth, could be an indication that cable bacteria are oxidizing
779 iron sulfides at that sediment depth and prevent their formation at shallower depths. Further,
780 cable bacteria have been found to directly compete with GSOB in transiently deoxygenated
781 systems, with cable bacteria active under oxygenated conditions and GSOB active in anoxic
782 conditions (Seitaj et al., 2015). Cable bacteria can also prevent the benthic release of sulfide,
783 which is toxic to many pelagic animals, via the creation of an iron-oxide buffer (formed through
784 Fe^{2+} oxidation) in near-surface sediments (Seitaj et al., 2015). Therefore, if cable bacteria activity
785 in the SBB decreased with declining oxygen concentrations below the sill, the iron oxide buffer
786 they create could have been reduced, encouraging the sulfate reduction zone to migrate towards
787 the sediment surface (as seen at NDT3-C). Cable bacteria can sometimes be detected in
788 sediments via a slight pH increase (typically pH > 8) (Schauer et al., 2014) which was not
789 reflected in our pH results, but this phenomenon is more typically seen in the laboratory and not
790 the field (Hermans et al., 2019).
791
792 **4.5 Iron and phosphate flux into SBB bottom water is a feature of transient deoxygenation.**
793
794 Release of dissolved iron and phosphate from sediment below anoxic waters is a well-
795 documented phenomenon (e.g., (Mortimer, 1941; Van Cappellen and Ingall, 1994; Van De
796 Velde et al., 2020; Noffke et al., 2012)) and this phenomenon is seen in the SBB as well. As
797 postulated previously (Kuwabara et al., 1999), basin flushing oxidizes iron sulfides at the
798 sediment-water interface, providing ample substrate for microbial iron reduction once anoxia
799 returns. This iron reduction initiates high rates of Fe^{2+} release from SBB depocenter sediment
800 (Fig. 5). Iron reduction further releases iron-bound PO_4^{3-} (Mortimer, 1941) as seen by high

benthic fluxes of PO_4^{3-} at the depocenter (Fig. 5), although notably some of this PO_4^{3-} release is likely attributed to organic matter degradation (Van Cappellen and Ingall, 1994). High benthic Fe^{2+} and PO_4^{3-} fluxes were also seen on the Peruvian shelf during transient anoxia (Noffke et al., 2012). The release of these solutes was interpreted to be sourced from a layer of reactive iron hydroxides existing near the sediment surface, likely established during a recent oxygenation event. Similar conditions, i.e., visibly oxidized (reddish) sediment laminae and a thin zone of iron reduction apparent from a peak in Fe^{2+} at the sediment-water interface, were found in sediment from the SBB depocenter. Deeper in the persistently anoxic core of the Peruvian OMZ, sediment appears to have little to no flux of $Fe^{2+}$and PO_4^{3-} into the bottom water (Noffke et al., 2012). Here, iron at the sediment-water interface is hypothesized to be locked up in iron sulfides, which are rarely re-oxidized due to persistent anoxia.

In a different study from the Eastern Gotland Basin in the Baltic Sea, enhanced elemental fluxes were observed during a decadal oxygen flushing event (Van De Velde et al., 2020), which was attributed to enhanced elemental recycling, or cycles of mineral precipitation in the water column followed by mineral dissolution once those minerals sink to the sediment. Notably, the iron flux observed in the Eastern Gotland Basin (max. 0.08 mmol m^{-2} d^{-1}) (Van De Velde et al., 2020) was two orders of magnitude lower than the flux observed in the anoxic depocenter of the Santa Barbara Basin (max. 4.9 mmol m^{-2} d^{-1}). It is further notable that benthic fluxes of PO_4^{3-} in the SBB depocenter were also an order of magnitude higher than fluxes in the Eastern Gotland Basin's hypoxic transition zone (3.6 vs. 0.23 mmol PO_4^{3-} m^{-2} d^{-1}) - both of which contained GSOB mats, but while the SBB was anoxic and the Eastern Gotland Basin was hypoxic (Noffke et al., 2016). These differences in Fe^{2+} and PO_4^{3}- flux between the SBB and the Eastern Gotland

824 Basin suggest that reoxidation of the sediment-water interface during basin flushing, as opposed
825 to water-column-associated reoxidation, appears to encourage higher benthic iron fluxes.
826
827 Fe^{2+} and PO_4^{3-} flux from the SBB depocenter were also approximately five times higher (Fig. 5)
828 compared to the anoxic Peruvian shelf (4.9 vs. 0.9 mmol Fe^{2+} m^{-2} d^{-1} and 3.6 vs. 0.8 mmol PO_4^{3-}
829 m^{-2} d^{-1}, respectively) (Noffke et al., 2012). Based on Fe^{2+} profiles, the zone of iron reduction in
830 Peruvian shelf sediments extended down to approx. 10 cm, while the zone appeared to be much
831 shallower and narrower (less than the top 5 cm) in the SBB depocenter. These differences in
832 magnitude of Fe^{2+} concentration and Fe^{2+} and PO_4^{3-} flux between the SBB depocenter and the
833 Peruvian shelf could be attributed to differences in the recency and magnitude of reoxygenation
834 events. The release of Fe^{2+} from sediment into the bottom water could create a buffer against
835 reoxygenation in transiently deoxygenated systems, giving a competitive advantage to anaerobic
836 benthic metabolisms (Dale et al., 2013; Wallmann et al., 2022). Additionally, both Fe^{2+} and
837 PO_4^{3-} release from the SBB sediment could allow for higher rates of primary productivity if
838 those constituents diffused into the photic zone (Robinson et al., 2022). The fate of Fe^{2+} and
839 PO_4^{3-} diffusing into SBB waters from the sediment-water interface is a focus of ongoing work
840 within the basin.
841
842 **5 Conclusions**
843
844 This research expands upon the wealth of science already conducted in the SBB and other
845 transiently deoxygenated environments by examining changes in benthic biogeochemistry
846 promoted by the onset of anoxia. Our main interpretations are summarized in Fig. 7. We found
847 that GSOB mats proliferate in the SBB where the bottom water is anoxic and nitrate

concentrations are declining (Fig. 7, A- and depocenter stations). Nitrate uptake by SBB sediment is similar regardless of GSOB mat presence, but these mats appear to initiate a shift from denitrification to DNRA as the primary nitrate reduction pathway (Fig. 7, beginning at B-stations). The zone of sulfate reduction rises to the sediment-water interface where GSOB mats are present (Fig. 7, A-stations), possibly because the hyper-accumulation of nitrate into their intracellular vacuoles starves the environment of this more powerful electron acceptor. However, following the natural order of electron acceptor utilization (Boudreau and Jorgensen, 2001), iron oxides near the sediment-water interface must be exhausted before sulfate reduction can dominate surface sediments and GSOB mats can proliferate in the SBB (Fig. 7, depocenter stations). If anoxic events become longer and more frequent in the SBB because of global warming (see, e.g., (Qin et al., 2022; Stramma et al., 2008)), the iron oxide buffer built up in shallower basin depths could be exhausted, allowing for surface sulfate reduction and the proliferation of GSOB mats in shallower margins of the basin than currently seen. Further, the same transient deoxygenation that allows for these mats to re-stablish themselves also allows for a high Fe^{2+} and PO_4^{3-} flux into the SBB water column. In order to fully understand the complex changes in the benthic environment in response to deoxygenation, genomic and molecular work of the upper sediment community needs to be characterized. Overall, the insights gleaned from this research will aid in the understanding of fundamental biogeochemical changes that occur when marine environments become anoxic.

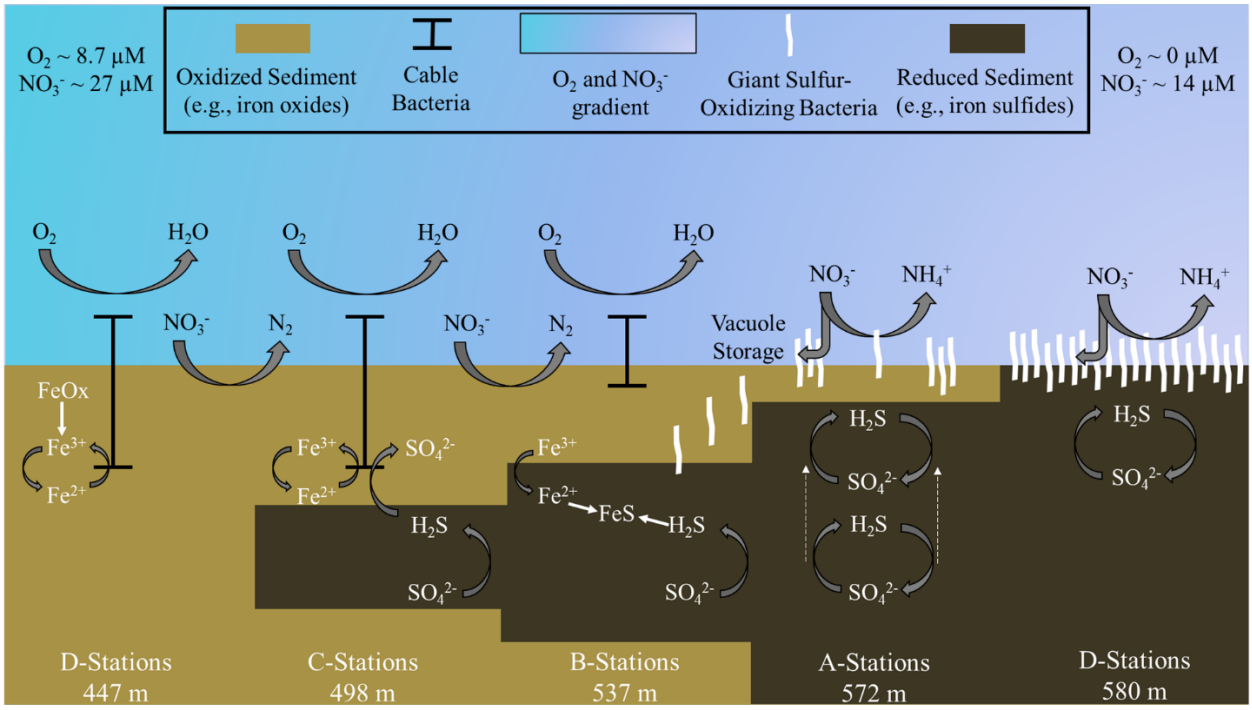

Figure 7: Schematic of biogeochemical processes in the Santa Barbara Basin along the depth gradients studied in October/November 2019. Teal to lavender gradient represents a decline in O_2 and NO_3^- concentrations with basin depth. In the shallower, hypoxic basin (D-stations), denitrification and iron reduction are dominant and reduced iron is rapidly re-oxidized in near-surface sediment by cable bacteria. Deeper in the basin (A-stations and depocenter), nitrogen cycling shifts towards dissimilatory nitrate reduction to ammonia (DNRA). Reduced iron combines with sulfide, produced by sulfate reduction, diffusing from deeper sediment layers to form iron sulfides. As oxygen concentration approaches zero between the A-stations and the basin's depocenter, giant sulfur-oxidizing bacteria hyper-accumulate nitrate in their intracellular vacuoles. Nitrate removal combined with the exhaustion of available iron oxides in the near-surface sediments allows the zone of sulfate reduction to migrate towards the surface (see dashed arrows at A-stations), providing the giant sulfur-oxidizing bacteria with sufficient reduced sulfur to proliferate into thick, contiguous mats. Note: Figure is not to scale, and processes are simplified to illustrate main concepts.

Acknowledgements

We thank the captain, crew, and scientific party of the R/V Atlantis, and the crew of the ROV Jason for their technical and logistical support during the research expedition AT42-19. We also thank Q. Qin, E. Arrington, M. O'Beirne, A. Mazariegos, X. Moreno, A. Eastman, and K. Gosselin for assisting with shipboard analyses. We thank J. Liu for assistance in reviewing the data processing for this manuscript. We further thank M. Alisch from the Max-Planck-Institute in Bremen, Germany for DIC analyses. We thank G. Eickert-Grötzschel, V. Hübner, A. Niclas, I. Schröder, and C. Wigand from the Max-Planck-Institute in Bremen, Germany for constructing the microsensors. We acknowledge J. Matthews from the UC Davis Stable Isotope facility for assisting with solid phase analyses. Funding for this work was provided by the US National Science Foundation, NSF OCE-1756947 and OCE-1830033 (to DLV) and OCE-1829981 (to TT), and a Simons Foundation Postdoctoral Fellowship in Marine Microbial Ecology (No. 547606 to XP). Further support was provided by the Max Planck Society and the Alfred Wegener Institute for Polar and Marine Research.

Data availability.

Biogeochemical data presented in this manuscript are accessible through the Biological & Chemical Oceanography Data Management Office (BCO-DMO) at the following landing pages: https://www.bco-dmo.org/dataset/867007; https://www.bco-dmo.org/dataset/867113; https://www.bco-dmo.org/dataset/867221; https://www.bco-dmo.org/dataset/896706

Author contributions.

TT, DV, FK, NL, and JT designed the project. DJY, SK, JT, DR, and TT processed sediment cores at sea. DJY conducted geochemical analyses of sediment porewater and benthic flux chamber water. DJY prepared TOC and TON samples. DR and SK analyzed sediment porosity and density. TT and SK performed shipboard sulfate reduction incubations. DJY and DR conducted sulfate reduction analyses. DJY, NL, and JT transformed and interpreted ROV Jason data. FJ and FW operated BFC and microprofilers and analyzed associated data. XP conducted ^{15}N experiments and analyses. All authors reviewed and edited the manuscript.

Competing interests.

At least one of the (co-)authors is a member of the editorial board of Biogeosciences.

References

Algar, C. K. and Vallino, J. J.: Predicting microbial nitrate reduction pathways in coastal sediments, Aquatic Microbial Ecology, 71, 223-238, 2014.

An, S. and Gardner, W. S.: Dissimilatory nitrate reduction to ammonium (DNRA) as a nitrogen link, versus denitrification as a sink in a shallow estuary (Laguna Madre/Baffin Bay, Texas), Marine Ecology Progress Series, 237, 41-50, 2002.

Bernhard, J. M., Visscher, P. T., and Bowser, S. S.: Submillimeter life positions of bacteria, protists, and metazoans in laminated sediments of the Santa Barbara Basin, Limnology and Oceanography, 48, 813-828, 2003.

Bernhard, J. M., Buck, K. R., Farmer, M. A., and Bowser, S. S.: The Santa Barbara Basin is a symbiosis oasis, Nature, 403, 77-80, 2000.

Bernhard, J. M., Casciotti, K. L., McIlvin, M. R., Beaudoin, D. J., Visscher, P. T., and Edgcomb, V. P.: Potential importance of physiologically diverse benthic foraminifera in sedimentary nitrate storage and respiration, Journal of Geophysical Research: Biogeosciences, 117, 2012.

Bograd, S. J., Schwing, F. B., Castro, C. G., and Timothy, D. A.: Bottom water renewal in the Santa Barbara Basin, Journal of Geophysical Research: Oceans, 107, 9-1-9-9, 2002.

Bonaglia, S., Nascimento, F. A., Bartoli, M., Klawonn, I., and Brüchert, V.: Meiofauna increases bacterial denitrification in marine sediments, Nature communications, 5, 5133, 2014.

Boudreau, B. P. and Jorgensen, B. B.: The benthic boundary layer: Transport processes and biogeochemistry, 2001.

Bourbonnais, A., Letscher, R. T., Bange, H. W., Echevin, V., Larkum, J., Mohn, J., Yoshida, N., and Altabet, M. A.: N2O production and consumption from stable isotopic and concentration data in the Peruvian coastal upwelling system, Global Biogeochemical Cycles, 31, 678-698, 2017.

Bremner, J.: Biogenic sediments on the South West African continental margin, 1981.

Brüchert, V., Jørgensen, B. B., Neumann, K., Riechmann, D., Schlösser, M., and Schulz, H.: Regulation of bacterial sulfate reduction and hydrogen sulfide fluxes in the central Namibian coastal upwelling zone, Geochim. Cosmochim. Acta, 67, 4505-4518, 2003.

Caffrey, J. M., Bonaglia, S., and Conley, D. J.: Short exposure to oxygen and sulfide alter nitrification, denitrification, and DNRA activity in seasonally hypoxic estuarine sediments, FEMS microbiology letters, 366, fny288, 2019.

California Cooperative Oceanic Fisheries Investigations: https://www.calcofi.org/ccdata.html, last

Canfield, D. E.: Reactive iron in marine sediments, Geochimica et cosmochimica acta, 53, 619-632, 1989.

Canfield, D. E., Stewart, F. J., Thamdrup, B., De Brabandere, L., Dalsgaard, T., Delong, E. F., Revsbech, N. P., and Ulloa, O.: A cryptic sulfur cycle in oxygen-minimum–zone waters off the Chilean coast, Science, 330, 1375-1378, 2010.

Charoenpong, C. N., Bristow, L. A., and Altabet, M. A.: A continuous flow isotope ratio mass spectrometry method for high precision determination of dissolved gas ratios and isotopic composition, Limnology and Oceanography: Methods, 12, 323-337, 2014.

Cline, J. D.: Spectrophometric determination of hydrogen sulfide in natural waters, Limnol. Oceanogr., 14, 454-458, 1969.
Dale, A. W., Bertics, V. J., Treude, T., and Wallmann, K.: Modeling benthic-pelagic nutrient exchange processes and porewater distributions in a seasonally hypoxic sediment: evidence for massive phosphate release by Beggiatoa?, Biogeosciences, 10, 629-651, 2013.
Dale, A. W., Sommer, S., Lomnitz, U., Bourbonnais, A., and Wallmann, K.: Biological nitrate transport in sediments on the Peruvian margin mitigates benthic sulfide emissions and drives pelagic N loss during stagnation events, Deep Sea Research Part I: Oceanographic Research Papers, 112, 123-136, 2016.
Dale, A. W., Sommer, S., Ryabenko, E., Noffke, A., Bohlen, L., Wallmann, K., Stolpovsky, K., Greinert, J., and Pfannkuche, O.: Benthic nitrogen fluxes and fractionation of nitrate in the Mauritanian oxygen minimum zone (Eastern Tropical North Atlantic), Geochimica et Cosmochimica Acta, 134, 234-256, 2014.
Dale, A. W., Sommer, S., Bohlen, L., Treude, T., Bertics, V. J., Bange, H. W., Pfannkuche, O., Schorp, T., Mattsdotter, M., and Wallmann, K.: Rates and regulation of nitrogen cycling in seasonally hypoxic sediments during winter (Boknis Eck, SW Baltic Sea): Sensitivity to environmental variables, Estuar. Continent. Shelf Sci., 95, 14-28, 2011.
Dale, A. W., Sommer, S., Lomnitz, U., Montes, I., Treude, T., Liebetrau, V., Gier, J., Hensen, C., Dengler, M., Stolpovsky, K., Bryant, L. D., and Wallmann, K.: Organic carbon production, mineralisation and preservation on the Peruvian margin, Biogeosciences, 12, 1537-1559, 2015.
De Brabandere, L., Bonaglia, S., Kononets, M. Y., Viktorsson, L., Stigebrandt, A., Thamdrup, B., and Hall, P. O.: Oxygenation of an anoxic fjord basin strongly stimulates benthic denitrification and DNRA, Biogeochemistry, 126, 131-152, 2015.
Emery, K., Hülsemann, J., and Rodolfo, K.: Influence of turbidity currents upon basin waters, Limnology and Oceanography, 7, 439-446, 1962.
Emmer, E. and Thunell, R. C.: Nitrogen isotope variations in Santa Barbara Basin sediments: Implications for denitrification in the eastern tropical North Pacific during the last 50,000 years, Paleoceanography, 15, 377-387, 2000.
Fossing, H., Gallardo, V. A., Jørgensen, B. B., Hüttel, M., Nielsen, L. P., Schulz, H., Canfield, D. E., Forster, S., Glud, R. N., and Gundersen, J. K.: Concentration and transport of nitrate by the mat-forming sulphur bacterium Thioploca, Nature, 374, 713-715, 1995.
García-Robledo, E., Corzo, A., and Papaspyrou, S.: A fast and direct spectrophotometric method for the sequential determination of nitrate and nitrite at low concentrations in small volumes, Marine Chemistry, 162, 30-36, 2014.
Gier, J., Sommer, S., Löscher, C. R., Dale, A. W., Schmitz, R. A., and Treude, T.: Nitrogen fixation in sediments along a depth transect through the Peruvian oxygen minimum zone, Biogeosciences, 13, 4065–4080, 2016.
Glud, R. N., Gundersen, J. K., and Ramsing, N. B.: Electrochemical and optical oxygen microsensors for in situ measurements, in: In situ monitoring of aquatic systems: Chemical analysis and speciation, edited by: Buffle, J., and Horvai, G., Wiley, 2000.

997 Goericke, R., Bograd, S. J., and Grundle, D. S.: Denitrification and flushing of the Santa Barbara
998 Basin bottom waters, Deep Sea Research Part II: Topical Studies in Oceanography, 112,
999 53-60, 2015.
1000 Grasshoff, K., Ehrhardt, M., and Kremling, K.: Methods of seawater analysis, Wiley-VCH Verlag
1001 GmbH, Weinheim1999.
1002 Gundersen, J. K. and Jørgensen, B. B.: Microstructure of diffusive boundary layers and the
1003 oxygen uptake of the sea floor, Nature, 345, 604-607, 1990.
1004 Hall, P. O. J. and Aller, R. C.: Rapid small-volume flow injection analysis for $\sum$ CO2 and NH4+ in
1005 marine and fresh waters, Limnol. Oceanogr., 37, 1113-1119, 1992.
1006 Hardison, A. K., Algar, C. K., Giblin, A. E., and Rich, J. J.: Influence of organic carbon and nitrate
1007 loading on partitioning between dissimilatory nitrate reduction to ammonium (DNRA)
1008 and N2 production, Geochimica et Cosmochimica Acta, 164, 146-160, 2015.
1009 Harris, D., Horwáth, W. R., and Van Kessel, C.: Acid fumigation of soils to remove carbonates
1010 prior to total organic carbon or carbon-13 isotopic analysis, Soil Science Society of
1011 America Journal, 65, 1853-1856, 2001.
1012 Hermans, M., Lenstra, W. K., Hidalgo-Martinez, S., van Helmond, N. A., Witbaard, R.,
1013 Meysman, F. J., Gonzalez, S., and Slomp, C. P.: Abundance and biogeochemical impact
1014 of cable bacteria in Baltic Sea sediments, Environmental science & technology, 53,
1015 7494-7503, 2019.
1016 Hossain, M., Bhattacharya, P., Frape, S. K., Jacks, G., Islam, M. M., Rahman, M. M., von
1017 Brömssen, M., Hasan, M. A., and Ahmed, K. M.: Sediment color tool for targeting
1018 arsenic-safe aquifers for the installation of shallow drinking water tubewells, Science
1019 of the Total Environment, 493, 615-625, 2014.
1020 Huettel, M., Forster, S., Kloser, S., and Fossing, H.: Vertical migration in the sediment-dwelling
1021 sulfur bacteria Thioploca spp. in overcoming diffusion limitations, Applied and
1022 Environmental Microbiology, 62, 1863-1872, 1996.
1023 Hylén, A., Bonaglia, S., Robertson, E., Marzocchi, U., Kononets, M., and Hall, P. O.: Enhanced
1024 benthic nitrous oxide and ammonium production after natural oxygenation of long-
1025 term anoxic sediments, Limnology and Oceanography, 67, 419-433, 2022.
1026 Høgslund, S., Revsbech, N. P., Kuenen, J. G., Jørgensen, B. B., Gallardo, V. A., Vossenberg, J. v.
1027 d., Nielsen, J. L., Holmkvist, L., Arning, E. T., and Nielsen, L. P.: Physiology and
1028 behaviour of marine Thioploca, The ISME journal, 3, 647-657, 2009.
1029 Jeroschewsky, P., Steuckart, C., and Kuehl, M.: An amperometric microsensor for the
1030 determination af H2S in aquatic environments, Anal. Chem., 68, 4351-4357, 1996.
1031 Jørgensen, B.: Distribution of colorless sulfur bacteria (Beggiatoa spp.) in a coastal marine
1032 sediment, Marine Biology, 41, 19-28, 1977.
1033 Jørgensen, B. B.: A comparison of methods for the quantification of bacterial sulphate
1034 reduction in coastal marine sediments: I. Measurements with radiotracer techniques,
1035 Geomicrobiol. J., 1, 11-27, 1978.
1036 Jørgensen, B. B. and Nelson, D. C.: Sulfide oxidation in marine sediments: Geochemistry meets
1037 microbiology, Geological Society of America, Special Paper 379, 63-81, 2004.

Kallmeyer, J., Ferdelman, T. G., Weber, A., Fossing, H., and Jørgensen, B. B.: A cold chromium distillation procedure for radiolabeled sulfide applied to sulfate reduction measurements, Limnol. Oceanogr. Methods, 2, 171-180, 2004.
Kamp, A., Høgslund, S., Risgaard-Petersen, N., and Stief, P.: Nitrate storage and dissimilatory nitrate reduction by eukaryotic microbes, Frontiers in microbiology, 6, 1492, 2015.
Kamp, A., de Beer, D., Nitsch, J. L., Lavik, G., and Stief, P.: Diatoms respire nitrate to survive dark and anoxic conditions, Proceedings of the National Academy of Sciences, 108, 5649-5654, 2011.
Kessler, A. J., Wawryk, M., Marzocchi, U., Roberts, K. L., Wong, W. W., Risgaard-Petersen, N., Meysman, F. J., Glud, R. N., and Cook, P. L.: Cable bacteria promote DNRA through iron sulfide dissolution, Limnology and Oceanography, 64, 1228-1238, 2019.
Kjeldsen, K. U., Schreiber, L., Thorup, C. A., Boesen, T., Bjerg, J. T., Yang, T., Dueholm, M. S., Larsen, S., Risgaard-Petersen, N., and Nierychlo, M.: On the evolution and physiology of cable bacteria, Proceedings of the National Academy of Sciences, 116, 19116-19125, 2019.
Kononets, M., Tengberg, A., Nilsson, M., Ekeroth, N., Hylén, A., Robertson, E. K., Van De Velde, S., Bonaglia, S., Rütting, T., and Blomqvist, S.: In situ incubations with the Gothenburg benthic chamber landers: Applications and quality control, Journal of Marine Systems, 214, 103475, 2021.
Kraft, B., Tegetmeyer, H. E., Sharma, R., Klotz, M. G., Ferdelman, T. G., Hettich, R. L., Geelhoed, J. S., and Strous, M.: The environmental controls that govern the end product of bacterial nitrate respiration, Science, 345, 676-679, 2014.
Kuwabara, J. S., van Geen, A., McCorkle, D. C., and Bernhard, J. M.: Dissolved sulfide distributions in the water column and sediment pore waters of the Santa Barbara Basin, Geochimica et Cosmochimica Acta, 63, 2199-2209, 1999.
Lazo-Murphy, B. M., Larson, S., Staines, S., Bruck, H., McHenry, J., Bourbonnais, A., and Peng, X.: Nitrous oxide production and isotopomer composition by fungi isolated from salt marsh sediments, Frontiers in Marine Science, 9, 1098508, 2022.
Levin, L. A., Gutierrez, D., Rathburn, A. E., Neira, C., Sellanes, J., Munoz, P., Gallardo, V. A., and Salamance, M.: Bethic processes on the Peru margin: a transect across the oxygen minimum zone during the 1997-98 El Nino, Prog. Oceanog., 53, 1-27, 2002.
Marchant, H. K., Lavik, G., Holtappels, M., and Kuypers, M. M.: The fate of nitrate in intertidal permeable sediments, PloS one, 9, e104517, 2014.
Marzocchi, U., Bonaglia, S., van de Velde, S., Hall, P. O., Schramm, A., Risgaard-Petersen, N., and Meysman, F. J.: Transient bottom water oxygenation creates a niche for cable bacteria in long-term anoxic sediments of the Eastern Gotland Basin, Environmental microbiology, 20, 3031-3041, 2018.
Marzocchi, U., Trojan, D., Larsen, S., Louise Meyer, R., Peter Revsbech, N., Schramm, A., Peter Nielsen, L., and Risgaard-Petersen, N.: Electric coupling between distant nitrate reduction and sulfide oxidation in marine sediment, The ISME journal, 8, 1682-1690, 2014.
Middelburg, J. and Levin, L.: Coastal hypoxia and sediment biogeochemistry, Biogeosciences, 6, 1273-1293, 2009.

Mortimer, C. H.: The exchange of dissolved substances between mud and water in lakes, Journal of ecology, 29, 280-329, 1941.
Mosch, T., Sommer, S., Dengler, M., Noffke, A., Bohlen, L., Pfannkuche, O., Liebetrau, V., and Wallmann, K.: Factors influencing the distribution of epibenthic megafauna across the Peruvian oxygen minimum zone, Deep Sea Research Part I: Oceanographic Research Papers, 68, 123-135, 2012.
Mußmann, M., Schulz, H. N., Strotmann, B., Kjær, T., Nielsen, L. P., Rosselló-Mora, R. A., Amann, R. I., and Jørgensen, B. B.: Phylogeny and distribution of nitrate-storing Beggiatoa spp. in coastal marine sediments, Environmental Microbiology, 5, 523-533, 2003.
Myhre, S. E., Pak, D., Borreggine, M., Kennett, J. P., Nicholson, C., Hill, T. M., and Deutsch, C.: Oxygen minimum zone biotic baseline transects for paleoceanographic reconstructions in Santa Barbara Basin, CA, Deep Sea Research Part II: Topical Studies in Oceanography, 150, 118-131, 2018.
Naik, R., Naqvi, S., and Araujo, J.: Anaerobic carbon mineralisation through sulphate reduction in the inner shelf sediments of eastern Arabian Sea, Estuaries and Coasts, 40, 134-144, 2017.
Noffke, A., Sommer, S., Dale, A., Hall, P., and Pfannkuche, O.: Benthic nutrient fluxes in the Eastern Gotland Basin (Baltic Sea) with particular focus on microbial mat ecosystems, Journal of Marine Systems, 158, 1-12, 2016.
Noffke, A., Hensen, C., Sommer, S., Scholz, F., Bohlen, L., Mosch, T., Graco, M., and Wallmann, K.: Benthic iron and phosphorus fluxes across the Peruvian oxygen minimum zone, Limnol. Oceanogr., 57, 851-867, 2012.
Pavlova, G. Y., Tishchenko, P. Y., Volkova, T., Dickson, A., and Wallmann, K.: Intercalibration of Bruevich's method to determine the total alkalinity in seawater, Oceanology, 48, 438-443, 2008.
Peng, X., Ji, Q., Angell, J. H., Kearns, P. J., Yang, H. J., Bowen, J. L., and Ward, B. B.: Long-term fertilization alters the relative importance of nitrate reduction pathways in salt marsh sediments, Journal of Geophysical Research: Biogeosciences, 121, 2082-2095, 2016.
Peng, X., Yousavich, D. J., Bourbonnais, A., Wenzhoefer, F., Janssen, F., Treude, T., and Valentine, D. L.: The fate of fixed nitrogen in Santa Barbara Basin sediments during seasonal anoxia, EGUsphere, 2023, 1-26, 2023.
Pfeffer, C., Larsen, S., Song, J., Dong, M., Besenbacher, F., Meyer, R. L., Kjeldsen, K. U., Schreiber, L., Gorby, Y. A., and El-Naggar, M. Y.: Filamentous bacteria transport electrons over centimetre distances, Nature, 491, 218-221, 2012.
Plass, A., Schlosser, C., Sommer, S., Dale, A. W., Achterberg, E. P., and Scholz, F.: The control of hydrogen sulfide on benthic iron and cadmium fluxes in the oxygen minimum zone off Peru, Biogeosciences, 17, 3685-3704, 2020.
Porubsky, W., Weston, N., and Joye, S.: Benthic metabolism and the fate of dissolved inorganic nitrogen in intertidal sediments, Estuarine, Coastal and Shelf Science, 83, 392-402, 2009.

Preisler, A., De Beer, D., Lichtschlag, A., Lavik, G., Boetius, A., and Jørgensen, B. B.: Biological and chemical sulfide oxidation in a Beggiatoa inhabited marine sediment, ISME Journal, 341-351, 2007.

Prokopenko, M., Hammond, D., Berelson, W., Bernhard, J., Stott, L., and Douglas, R.: Nitrogen cycling in the sediments of Santa Barbara basin and Eastern Subtropical North Pacific: Nitrogen isotopes, diagenesis and possible chemosymbiosis between two lithotrophs (Thioploca and Anammox)—"riding on a glider", Earth and Planetary Science Letters, 242, 186-204, 2006.

Qin, Q., Kinnaman, F. S., Gosselin, K. M., Liu, N., Treude, T., and Valentine, D. L.: Seasonality of Water Column Methane Oxidation and Deoxygenation in a Dynamic Marine Environment, Geochimica et Cosmochimica Acta, 2022.

Raiswell, R. and Canfield, D. E.: The iron biogeochemical cycle past and present, Geochemical perspectives, 1, 1-2, 2012.

Reimers, C. E., Ruttenberg, K. C., Canfield, D. E., Christiansen, M. B., and Martin, J. B.: Porewater pH and authigenic phases formed in the uppermost sediments of Santa Barbara Basin, Geochim. Cosmochim. Acta, 60, 4037-4057, 1996.

Revsbech, N. P. and Jørgensen, B. B.: Microelectrodes: their use in microbial ecology, in: Adv. Microb. Ecol., edited by: Marshall, K. C., Plenum, New York, 293-352, 1986.

Risgaard-Petersen, N., Langezaal, A. M., Ingvardsen, S., Schmid, M. C., Jetten, M. S. M., Op den Camp, H. J. M., Derksen, J. W. M., Pina-Ochoa, E., Eriksson, S. P., Nielsen, L. P., Revsbech, N. P., Cedhagen, T., and Zwaan van der, G. J.: Evidence for complete denitrification in a benthic foraminifer, Nature, 443, 93-96, 2006.

Robinson, D. M., Pham, A. L., Yousavich, D. J., Janssen, F., Wenzhöfer, F., Arrington, E. C., Gosselin, K. M., Sandoval-Belmar, M., Mar, M., and Valentine, D. L.: Iron "Ore" Nothing: Benthic iron fluxes from the oxygen-deficient Santa Barbara Basin enhance phytoplankton productivity in surface waters, Biogeosciences Discussions, 1-36, 2022.

Sayama, M.: Presence of nitrate-accumulating sulfur bacteria and their influence on nitrogen cycling in a shallow coastal marine sediment, Applied and Environmental Microbiology, 67, 3481-3487, 2001.

Schauer, R., Risgaard-Petersen, N., Kjeldsen, K. U., Tataru Bjerg, J. J., B Jørgensen, B., Schramm, A., and Nielsen, L. P.: Succession of cable bacteria and electric currents in marine sediment, The ISME journal, 8, 1314-1322, 2014.

Schroller-Lomnitz, U., Hensen, C., Dale, A. W., Scholz, F., Clemens, D., Sommer, S., Noffke, A., and Wallmann, K.: Dissolved benthic phosphate, iron and carbon fluxes in the Mauritanian upwelling system and implications for ongoing deoxygenation, Deep Sea Research Part I: Oceanographic Research Papers, 143, 70-84, 2019.

Schulz, H. N. and Schulz, H. D.: Large sulfur bacteria and the formation of phosphorite, Science, 307, 416-418, 2005.

Schulz, H. N., Jorgensen, B. B., Fossing, H. A., and Ramsing, N. B.: Community structure of filamentous, sheath-building sulfur bacteria, Thioploca spp., off the coast of Chile, Applied and Environmental Microbiology, 62, 1855-1862, 1996.

Schulz, H. N., Brinkhoff, T., Ferdelman, T. G., Hernández Mariné, M., Teske, A., and Jørgensen, B. B.: Dense populations of a giant sulfur bacterium in Namibian shelf sediments, Science, 284, 493-495, 1999.

Seitaj, D., Schauer, R., Sulu-Gambari, F., Hidalgo-Martinez, S., Malkin, S. Y., Burdorf, L. D., Slomp, C. P., and Meysman, F. J.: Cable bacteria generate a firewall against euxinia in seasonally hypoxic basins, Proceedings of the National Academy of Sciences, 112, 13278-13283, 2015.

Sholkovitz, E.: Interstitial water chemistry of the Santa Barbara Basin sediments, Geochimica et Cosmochimica Acta, 37, 2043-2073, 1973.

Sholkovitz, E. R. and Gieskes, J. M.: A PHYSICAL-CHEMICAL STUDY OF THE FLUSHING OF THE SANTA BARBARA BASIN 1, Limnology and Oceanography, 16, 479-489, 1971.

Sigman, D. M., Robinson, R., Knapp, A., Van Geen, A., McCorkle, D., Brandes, J., and Thunell, R.: Distinguishing between water column and sedimentary denitrification in the Santa Barbara Basin using the stable isotopes of nitrate, Geochemistry, Geophysics, Geosystems, 4, 2003.

Sommer, S., Gier, J., Treude, T., Lomnitz, U., Dengler, M., Cardich, J., and Dale, A. W.: Depletion of oxygen, nitrate and nitrite in the Peruvian oxygen minimum zone cause an imbalance of benthic nitrogen fluxes, Deep-Sea Res. I, 112, 113–122, 2016.

Stramma, L., Johnson, G. C., Sprintall, J., and Mohrholz, V.: Expanding oxygen-minimum zones in the tropical oceans, Science, 320, 655-658, 2008.

Sverdrup, H. and Allen, W.: Distribution of diatoms in relation to the character of water masses and currents off Southern California in 1938, J. mar. Res, 2, 131-144, 1939.

Thunell, R. C.: Particle fluxes in a coastal upwelling zone: sediment trap results from Santa Barbara Basin, California, Deep Sea Research Part II: Topical Studies in Oceanography, 45, 1863-1884, 1998.

Tiedje, J. M., Sexstone, A. J., Myrold, D. D., and Robinson, J. A.: Denitrification: ecological niches, competition and survival, Antonie van Leeuwenhoek, 48, 569-583, 1983.

Treude, T.: Biogeochemical reactions in marine sediments underlying anoxic water bodies, in: Anoxia: Paleontological Strategies and Evidence for Eukaryote Survival, edited by: Altenbach, A., Bernhard, J., and Seckbach, J., Cellular Origins, Life in Extreme Habitats and Astrobiology (COLE) Book Series, Springer, Dordrecht, 18-38, 2011.

Treude, T., Hamdan, L. J., Lemieux, S., Dale, A. W., and Sommer, S.: Rapid sulfur cycling in sediments from the Peruvian oxygen minimum zone featuring simultaneous sulfate reduction and sulfide oxidation, Limnology and Oceanography, 66, 2661-2671, 2021.

Treude, T., Smith, C. R., Wenzhoefer, F., Carney, E., Bernardino, A. F., Hannides, A. K., Krueger, M., and Boetius, A.: Biogeochemistry of a deep-sea whale fall: sulfate reduction, sulfide efflux and methanogenesis, Mar. Ecol. Prog. Ser., 382, 1-21, 2009.

Valentine, D. L., Fisher, G. B., Pizarro, O., Kaiser, C. L., Yoerger, D., Breier, J. A., and Tarn, J.: Autonomous marine robotic technology reveals an expansive benthic bacterial community relevant to regional nitrogen biogeochemistry, Environmental science & technology, 50, 11057-11065, 2016.

Van Cappellen, P. and Ingall, E. D.: Benthic phosphorus regeneration, net primary production, and ocean anoxia: A model of the coupled marine biogeochemical cycles of carbon and phosphorus, Paleoceanography, 9, 677-692, 1994.

Van De Velde, S., Lesven, L., Burdorf, L. D., Hidalgo-Martinez, S., Geelhoed, J. S., Van Rijswijk, P., Gao, Y., and Meysman, F. J.: The impact of electrogenic sulfur oxidation on the

biogeochemistry of coastal sediments: A field study, Geochimica et Cosmochimica Acta, 194, 211-232, 2016.
van de Velde, S. J., Hylén, A., Eriksson, M., James, R. K., Kononets, M. Y., Robertson, E. K., and Hall, P. O.: Exceptionally high respiration rates in the reactive surface layer of sediments underlying oxygen-deficient bottom waters, Proceedings of the Royal Society A, 479, 20230189, 2023.
van de Velde, S. J., Hylén, A., Kononets, M., Marzocchi, U., Leermakers, M., Choumiline, K., Hall, P. O., and Meysman, F. J.: Elevated sedimentary removal of Fe, Mn, and trace elements following a transient oxygenation event in the Eastern Gotland Basin, central Baltic Sea, Geochimica et Cosmochimica Acta, 271, 16-32, 2020.
Wallmann, K., José, Y. S., Hopwood, M. J., Somes, C. J., Dale, A. W., Scholz, F., Achterberg, E. P., and Oschlies, A.: Biogeochemical feedbacks may amplify ongoing and future ocean deoxygenation: a case study from the Peruvian oxygen minimum zone, Biogeochemistry, 159, 45-67, 2022.
Ward, B., Devol, A., Rich, J., Chang, B., Bulow, S., Naik, H., Pratihary, A., and Jayakumar, A.: Denitrification as the dominant nitrogen loss process in the Arabian Sea, Nature, 461, 78-81, 2009.
Zhang, L., Altabet, M. A., Wu, T., and Hadas, O.: Sensitive measurement of NH4+ 15N/14N (δ15NH4+) at natural abundance levels in fresh and saltwaters, Analytical Chemistry, 79, 5297-5303, 2007.
Zopfi, J., Kjær, T., Nielsen, L. P., and Jørgensen, B. B.: Ecology of Thioploca spp.: nitrate and sulfur storage in relation to chemical microgradients and influence of Thioploca spp. on the sedimentary nitrogen cycle, Applied and Environmental Microbiology, 67, 5530-5537, 2001.